Med Chem Res (2016) 25:769–789
DOI 10.1007/s00044-016-1527-9

MEDICINAL CHEMISTRY RESEARCH

ORIGINAL RESEARCH

Synthesis, crystal structure, biological evaluation, electronic aspects of hydrogen bonds, and QSAR studies of some new *N*-(substituted phenylurea) diazaphosphore derivatives as anticancer agents

Niloufar Dorosti[1] · Bahram Delfan[2] · Khodayar Gholivand[3] · Ali Asghar Ebrahimi Valmoozi[3]

Received: 1 October 2015 / Accepted: 4 February 2016 / Published online: 18 February 2016
© Springer Science+Business Media New York 2016

Abstract A new series of 2-[*N*-(*R*-phenylureido)]-1,3,2-diazaphosphore-2-oxide derivatives ($R = CH_3$, F, NO_2, CN) were synthesized and characterized by ^{31}P, ^{1}H, ^{13}C NMR and FT-IR spectral techniques. All the compounds were evaluated for their antibacterial activity against some Gram-positive, Gram-negative strains of bacteria, as well as for their cytotoxic effects on MCF-7, MDA-MB-231, PC-3, HeLa, and K562 human cell lines. In vitro activity results exhibited an important role for six-membered diaza ring in both assays as well as high effect of *meta*-methyl and *ortho*-fluoro substitutes on the aromatic ring against the studied human cell lines and *B. subtilis* bacteria, respectively. To understand the correlation between the anticancer activity and physicochemical properties of the synthesized compounds, the QSAR studies were carried out. Further, the crystal structure of compound **15** was investigated and revealed that the title derivative is composed of two symmetrically independent molecules in the solid state with *anti* configuration the C=O *versus* P=O. NBO and AIM analyses were performed to investigate electronic aspects of hydrogen bonding of the crystal cluster, which play an extremely important role in biochemical systems.

Keywords Diazaphosphore · Anticancer · Antibacterial · QSAR · AIM · NBO

Introduction

The increasing issue of drug resistance has prompted an intensive search for new bioactive agents. Phosphor heterocyclic compounds are attractive in this regard because structural properties of these derivatives such as steric, electronic, and conformational interactions allow them to interact easily with the biopolymers of the living systems (Hua *et al*., 2009; Venkatachalam *et al*., 2006; Mohe *et al*., 2003). They inhibit acetylcholinesterase and butyrylcholinesterase enzymes (Elgorashi *et al*., 2006; Gholivand *et al*., 2014) and, as such, are useful for inhibiting of cell proliferation in the treatment of cancer (Voorde *et al*., 2011; Monteil *et al*., 2014; Gholivand *et al*., 2010). In addition, these compounds exhibit antimicrobial, antimalarial, and antiviral activities (Gholivand and Dorosti, 2013; Mara *et al*., 2011; Hocková *et al*., 2011). One representative phosphor group is oxazaphosphorine family, which is used as potent drugs in the treatment of human cancers (Fig. 1a) (Li *et al*., 2003; Borch and Canute, 1991; Ludeman *et al*., 1979). Modification of cyclophosphamide (**CP**), one of oxazaphosphorinane derivatives, has led to the synthesis of numerous phosphoramidate alkylating agents (Venkatachalam *et al*., 2006; Li *et al*., 2003; Moon *et al*., 1995) to find an antitumor agent that has fewer side effects than drugs now present. In all the research, analogs of **CP** have two important components including *P* ring and the substituent on phosphor (Jiang *et al*., 2006; Sun

Electronic supplementary material The online version of this article (doi:10.1007/s00044-016-1527-9) contains supplementary material, which is available to authorized users.

✉ Niloufar Dorosti
nilufardorosti@gmail.com

[1] Department of Chemistry, Lorestan University, Khoramabad 68135-465, Iran

[2] Razi Herbal Medicines Research Center, Lorestan University of Medical Sciences, Khoramabad, Iran

[3] Department of Chemistry, Tarbiat Modares University, P.O. Box 14115-175, Tehran, Iran

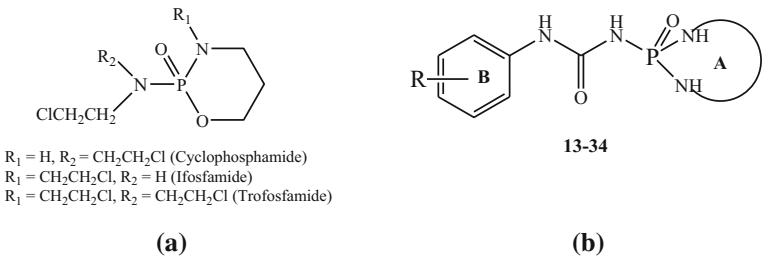

Fig. 1 **a** Bioactive oxazaphosphorines, **b** designed diazaphosphore

et al., 2006). In our previous studies, we have designed **CP** analogs based on the principle of conjugating the two pharmacophores of the phosphoryl and urea, with anticipation that the obtained hybrids could possess powerful biological activity (Gholivand *et al*., 2010, 2012). Our findings highlighted the importance of –NHC(O)NHP(O)– framework. In this paper, we describe the design and synthesis of **22** compounds with the general skeleton of $RC_6H_5NHC(O)NHP(O)(NH)^1(NH)^2$ (Fig. 1b). New desired derivatives **15**, **17**–**19**, **22**, **24**–**34** were characterized by IR, ^{1}H, ^{13}C, and ^{31}P NMR. Cytotoxic activities of **22** compounds, phenylurea, and standard drug (**CP**) were assayed against HeLa, PC-3, K562, MCF-7, and MDA-MB-231 human cancer cell lines to elucidate the importance of replacement of the 5- and 6-membered diazaphosphore rings (**A-ring**) instead of oxazaphosphorinane ring as well as the variation in the type of substituent and their position on the aromatic ring (**B-ring**). In the following, the selected compounds were screened for their antimicrobial activities. We also present quantitative structure–activity relationship (QSAR) studies for validation of the observed pharmacological properties of the investigated anticancer compounds and for determination of the most important parameters controlling these properties. In addition, the crystal structure of compound **15** was investigated and employed as reference for quantum mechanical (QM) calculations at the B3LYP level. It is well known that the hydrogen bond plays a key role in the chemistry of life, such as protein–ligand interactions and enzymatic activity (Jeffrey and Saenger, 1991; Carletti *et al*., 2010; Massiah *et al*., 2001). Moreover, the physicochemical properties of compounds depend on the presence of intermolecular hydrogen bonds. Hence, the electronic aspects of hydrogen bonds in the crystal structure of the compound **15** have been investigated by NBO and AIM analyses.

Experimental

Chemistry

^{1}H, ^{13}C, and ^{31}P spectra were recorded on a Bruker Avance DRX 500 spectrometer. ^{1}H and ^{13}C chemical shifts were determined relative to internal TMS, and ^{31}P chemical shifts, relative to 85 % H_3PO_4 as an external standard. IR spectra were recorded on a Shimadzu model IR-60 spectrometer using KBr pellets. Melting points were obtained with an electrothermal instrument.

*General procedure for the synthesis of diazaphosphorinanes **15**, **17**–**19**, and **22***

To a suspension of related intermediates of **2**–**12** (6 mmol) in dry diethyl ether (20 mL), 2, 2-dimethyl-1, 3-diaminopropane (1.23 g, 12.0 mmol) at 0 °C was added with stirring. After 5 h, the products were filtered off and washed with H_2O.

*5,5-Dimethyl-2-(N-4-fluoro-phenylureido)-1,3,2-diazaphosphorinane-2-oxide (**15**)* Yield: 60 %, m.p. 198–199 °C. ^{1}H NMR (500.13 MHz, d_6-DMSO) δ 0.78 (s, 3H, CH_3), 1.03 (s, 3H, CH_3), 2.57 (ddd, ^2J(H, H) = 12.00 Hz, ^3J(H, H) = 5.30 Hz, ^3J(P, H) = 24.4 Hz, 2H, CH), 2.98 (dd, ^2J(H, H) = 8.4 Hz, ^3J(H, H) = 3.65 Hz, 2H, CH), 4.67 (d,^{2}(P, H) = 3.8 Hz, 2H, $NH_{endocyclic}$), 7.08 (t, ^3J(H, H) = 8.85 Hz, 2H, Ar–H), 7.38 (dd, ^3J(H, H) = 9.00 Hz, ^3J(H, F) = 4.90 Hz, 2H, Ar–H), 7.68 (s, 1H, NHP), 9.37 (s, 1H, 4-F-C_6H_4NH) ppm; ^{13}C NMR (d_6-DMSO): δ 23.31 (s, CH_3), 24.88 (s, CH_3), 30.49 (d, ^3J(P, C) = 4.2 Hz, CH_2), 52.39 (d, ^2J(P, C) = 1.40 Hz, CH_2), 115.25 (d, ^1J(F, C) = 22.2 Hz, CH_2), 119.8 (d, ^2J(C, F) = 7.68 Hz), 135.7 (s), 153.49 (d, ^2J(P, C) = 2.38 Hz), 156.4 (s); ^{31}P NMR (202.46 MHz, d_6-DMSO) δ 3.72 (m). IR (KBr, cm^{-1}): 3215 (νN–H), 3112, 1690 (νC=O), 1614, 1569, 1468, 1446, 1310, 1337, 1220, 1178 (νP=O), 1090, 1046 (νP–N), 954 (νP–N), 864, 829, 766.

*5,5-Dimethyl-2-(N-4-cyano-phenylureido)-1,3,2-diazaphosphorinane-2-oxide (**17**)* Yield: 65 %, m.p. 192–193 °C. ^{1}H NMR (500.13 MHz, d_6-DMSO) δ 0.74 (s, 3H, CH_3), 1.03 (s, 3H, CH_3), 2.59 (ddd, ^2J(H, H) = 11.95 Hz, ^3J(H, H) = 5.15 Hz, ^3J(P, H) = 24.36 Hz, 2H, CH), 3.0 (d, ^3J(H, H) = 11.95 Hz, 2H, CH), 4.7 (d, ^2J(P, H) = 2.5 Hz, 2H, $NH_{endocyclic}$), 7.2 (d, ^3J(H, H) = 8.7 Hz, 2H, Ar–H), 7.41 (d, ^3J(H, H) = 8.7 Hz, 2H, Ar–H), 7.75 (d, ^2J(P, H) = 3.65 Hz, 1H, NHP), 9.47 (s, 1H, 4-CN-C_6H_4NH) ppm; ^{13}C NMR (d_6-DMSO): δ 23.29 (s, CH_3), 24.87 (s, CH_3), 30.47 (d, ^3J(P, C) = 4.33 Hz), 52.38 (s), 119.64 (s), 125.48 (s), 128.61 (s),

138.35 (s), 153.39 (d, ^2J(P, C) = 1.94 Hz). ^{31}P NMR (202.46 MHz, d_6-DMSO) δ 3.60 (m). IR (KBr, cm^{-1}): 3295 (νN–H), 1709 (νC=O), 1595, 1527, 1467, 1409, 1314, 1257, 1187(νP=O), 1089, 1044 (νP–N), 850, 761, 733, 545.

5,5-Dimethyl-2-(N-3-methyl-phenylureido)-1, 3, 2-diazaphosphorinane-2-oxide ***(18)*** Yield: 53 %, m.p. 163–164 °C. ^{1}H NMR (500.13 MHz, d_6-DMSO) δ 0.79 (s, 3H, CH_3), 1.03 (s, 3H, CH_3), 2.18 (s, 3H, CH_3), 2.56 (m, 2H, CH_2), 2.98 (m, 2H, CH_2), 4.74 (s, 2H, NH), 6.89 (m, 1H, Ar–H), 7.11 (m, 2H, Ar–H), 7.91 (d, 1H, NHP), 9.19 (s, 1H, 3-CH_3-C_6H_4NH). ^{13}C NMR (125.76 MHz, d_6-DMSO) δ 17.79 (s,CH_3), 23.36 (s, CH_3), 24.89 (s), 30.54 (d, ^3J(P, C) = 3.5 Hz), 52.21 (s), 119.93 (s), 122.26 (s), 126.08 (s), 126.49 (s), 130.02 (s), 137.49 (s), 153.44 (d, ^2J(P, C) = 2.54 Hz). ^{31}P NMR (202.46 MHz, d_6-DMSO) δ 4.62 (m) ppm. IR (KBr, cm^{-1}): 3320 (νN–H), 1680 (νC=O), 1616, 1588, 1558, 1455, 1326, 1193 (νP=O), 1099, 1038, 953, 861, 764, 607.

5, 5-dimethyl-2-(N-3-fluoro-phenylureido)-1, 3, 2-diazaphosphorinane-2-oxide ***(19)*** Yield: 60 %, m.p. 198–199 °C. ^{1}H NMR (500.13 MHz, d_6-DMSO) δ 0.78 (s, 3H, CH_3), 1.03 (s, 3H, CH_3), 2.58 (dd, ^2J(H, H) = 12.69 Hz, ^3J(H, H) = 5.30 Hz, 2H, CH), 2.96 (d, ^2J(H, H) = 11.4 Hz, 2H, CH), 4.69 (s, 2H, $NH_{endocyclic}$), 7.08 (t, ^3J(H, H) = 8.6 Hz, 2H, Ar–H), 7.37 (b, 2H, Ar–H), 7.7 (d, 1H, ^2J(P, H) = 5.18 Hz, NHP), 9.35 (s, 1H, 4-F-C_6H_4NH) ppm; ^{13}C NMR (d_6-DMSO): δ 23.28 (s, CH_3), 24.87 (s, CH_3), 30.46 (d, ^2J(P, C) = 4.5 Hz, CH_2), 52.38 (s), 115.12 (s), 115.41 (s), 119.82 (d, ^2J(C, F) = 7.7 Hz), 135.69 (d, ^2J(P, C) = 1.97 HZ), 153.49 (d, ^2J(P, C) = 2.49 Hz); ^{31}P NMR (202.46 MHz, d_6-DMSO) δ 3.8 (m). IR (KBr, cm^{-1}): 3215 (νN–H), 1690 (νC=O), 1614, 1569, 1468, 1446, 1337, 1220, 1178(νP=O), 1090, 1046 (νP–N), 954 (νP–N), 864, 829, 766.

5,5-Dimethyl-2-(N-2-fluoro-phenylureido)-1,3,2-diazaphosphorinane-2-oxide ***(22)*** Yield: 50 %, m.p. 198-199 °C. ^{1}H NMR (500.13 MHz, d_6-DMSO) δ 0.78 (s, 3H, CH_3), 1.02 (s, 3H, CH_3), 2.59 (ddd, ^2J(H, H) = 12.4 Hz, ^3J(H, H) = 5.27 Hz, ^3J(P, H) = 24.38 Hz, 2H, CH), 3.0 (d, ^2J(H, H) = 12.0 Hz, 2H, CH), 4.69 (d, ^2J(P, H) = 3.28 Hz, 2H, $NH_{endocyclic}$), 7.09 (t, ^3J(H, H) = 8.76 Hz, 2H, Ar–H), 7.38 (dd, ^3J(H, H) = 8.46 Hz, ^3J(H, H) = 5.1 Hz, 2H, Ar–H), 7.67 (d, ^2J(P, H) = 7.1 Hz, 1H, NHP), 9.35 (s, 1H, 2-F-C_6H_4NH) ppm; ^{13}C NMR (d_6-DMSO): δ 23.34 (s, CH_3), 24.94 (s, CH_3), 30.5 (d, ^3J(P, C) = 4.5 Hz, CH_2), 52.4 (s), 115.2 (s), 115.5 (s), 119.86 (d, ^2J(C, F) = 7.8 Hz), 135.72 (s), 153.53 (d, ^2J(P, C) = 2.57 Hz); ^{31}P NMR (202.46 MHz, d_6-DMSO) δ 3.79 (m). IR (KBr, cm^{-1}): 3215 (νN–H), 1690 (νC=O), 1614, 1569, 1468, 1446, 1337, 1220, 1178(νP=O), 1090, 1046 (νP–N), 954 (νP–N), 864, 829, 766.

General procedure for the synthesis of diazaphospholanes ***24–34***

These compounds were synthesized from the reaction of (6.06 mmol) intermediates **2–12** suspended in 10 mL dichloromethane with (0.73 g, 12.12 mmol) ethylenediamine at 0 °C. The solution was stirred overnight at room temperature and then evaporated in vacuum. The residue was washed with cooled water, and the precipitate was filtered off and dried at room temperature.

2-(N-phenylureido)-1,3,2-diazaphospholane-2-oxide ***(24)*** Yield: 50 %, m.p. 200–201 °C. ^{1}H NMR (500.13 MHz, d_6-DMSO) δ 3.12 (d, ^3J(P, H) = 5.05 Hz, 2H, CH_2), 3.27 (d, ^3J(P, H) = 7.1 Hz, 2H, CH_2), 4.74 (d, ^2J(P, H) = 12.5 Hz, 2H, NH), 6.95 (t, ^3J(H, H) = 7.35 Hz, 1H, CH), 7.24 (t, ^3J(H, H) = 8.8 Hz, 2H, CH, Ar–H), 7.36 (d, ^3J(H, H) = 7.7 Hz, 2H, CH, Ar–H), 7.52 (s, 1H, NHP), 9.52 (s, 1H, C_6H_5NH). ^{13}C NMR (125.76 MHz, d_6-DMSO) δ 40.8 (d, ^2J(P, C) = 11.52 Hz), 118.1 (s), 121.9 (s), 128.7 (s), 139.3 (s), 153.0 (d, ^2J(P, C) = 2.3 Hz). ^{31}P NMR (202.46 MHz, d_6-DMSO) δ 23.54 (m). IR (KBr, cm^{-1}): 3365 (νNH), 1695 (νC=O), 1600, 1540, 1482, 1443, 1409, 1309, 1285, 1213, 1155 (νP=O), 1103, 1083, 1057, 1027, 938, 847, 816, 776, 738, 689, 610, 557, 469.

2-(N-4-methyl-phenylureido)-1,3,2-diazaphospholane-2-oxide ***(25)*** Yield: 80 %, m.p. 189–190 °C. ^{1}H NMR (500.13 MHz, d_6-DMSO) δ 2.20 (s, 3H, CH_3), 3.12 (d, ^3J(P, H) = 12.65 Hz, 2H, CH_2), 3.26 (d, ^3J(P, H) = 7.4 Hz, 2H, CH_2), 4.71 (d, ^2J(P, H) = 12.35 Hz, 2H, $NH_{endocyclic}$), 7.04 (d, ^3J(H, H) = 8.20 Hz, 2H, CH, Ar–H), 7.25 (d, ^3J(H, H) = 8.20 Hz, 2H, CH, Ar–H), 7.50 (d, ^2J(P, H) = 6.00 Hz, 1H, NHP), 9.42 (s, 1H, 4-CH_3-C_6H_4 NH).^{13}C NMR (125.76 MHz, d_6-DMSO) δ 20.2 (s), 40.8 (d, ^2J(P, C) = 11.53 Hz), 118.2 (s), 129.1 (s), 130.8 (s), 136.7 (s), 153.0 (d, ^2J(P, C) = 2.454 Hz).^{31}P NMR (202.46 MHz, d_6-DMSO) δ 23.65 (m). IR (KBr, cm^{-1}): 3385 (νN–H), 3255, 2900, 1694 (νC=O), 1599, 1536, 1490, 1404, 1281, 1211, 1159 (νP=O), 1059 (νP–N), 940 (νP–N), 809 (νP–N), 719, 464.

2-(N-4-fluoro-phenylureido)-1,3,2-diazaphospholane-2-oxide ***(26)*** Yield: 70 %, m.p. 201–202 °C. ^{1}H NMR (500.13 MHz, d_6-DMSO) δ 3.26 (d, ^3J(P, H) = 12.0 Hz, 2H, CH_2), 3.27 (d, ^3J(P, H) = 7.8 Hz, 2H, CH_2), 4.75 (d, ^2J(P, H) = 12.3 Hz, 2H, $NH_{endocyclic}$), 7.08 (t, ^3J(H, H) = 8. 0 Hz, 2H, Ar–H), 7.38 (m, 2H, Ar–H), 7.58 (s, 1H, NHP), 9.55 (s, 1H, 4-F-C_6H_4NH). ^{13}C NMR (125.76 MHz, d_6-DMSO) δ 40.88 (d, ^2J(P, C) = 11.55 Hz), 115.25 (d, ^1J(C, F) = 22.2 Hz), 119.87 (d, ^2J(P, C) = 7.6 Hz), 135.64 (s), 153.14 (d, ^2J(P, C) = 1.89 Hz), 156.43 (s).^{31}P NMR (202.46 MHz, d_6-DMSO) δ 23.58 (m). IR (KBr, cm^{-1}): 3390(νN–H), 3250, 2955, 1701 (νC=O), 1612,

1546, 1509, 1484, 1405, 1292, 1217, 1153 (*v*P=O), 1101, 1055 (*v*P–N), 939, 825, 783, 747, 708, 460.

2-(N-4-nitro-phenylureido)-1,3,2-diazaphospholane-2-oxide ***(27)*** Yield: 70 %, m.p. 195–196 °C. ^{1}H NMR (500.13 MHz, d_6-DMSO) δ 3.16 (d, ^{3}J(P, H) = 12.5 Hz, 2H, CH_2), 3.29 (d, ^{3}J(P, H) = 7.65 Hz, 2H, CH_2), 4.83 (d, ^{2}J(P, H) = 12.8 Hz, 2H, $NH_{endocyclic}$), 7.62 (d, ^{3}J(H, H) = 9.05 Hz, 2H, Ar–H), 7.83 (s, 1H, NHP), 8.14 (d, ^{3}J(H, H) = 9.00 Hz, 2H, Ar–H), 10.19 (s, 1H, 4-NO_2-C_6H_4NH). ^{13}C NMR (125.76 MHz, d_6-DMSO) δ 40.8 (d, ^{2}J(P, C) = 11.78 Hz), 117.6 (s), 125.1 (s), 141.3 (s), 145.7 (s), 152.8 (d, ^{2}J(P, C) = 2.64 Hz).^{31}P NMR (202.46 MHz, d_6-DMSO) δ 23.30 (m). IR (KBr, cm^{-1}): 3375 (*v*NH), 3265, 2960, 1705 (*v*C=O), 1549, 1489, 1407, 1328 (νNO_2), 1299, 1155 (*v*P=O), 1059 (*v*P–N), 940 (*v*P–N), 847 (*v*P–N), 809, 732.

2-(N-4-cyano-phenylureido)-1,3,2-diazaphospholane-2-oxide ***(28)*** Yield: 73 %, m.p. 192–193 °C. ^{1}H NMR (500.13 MHz, d_6-DMSO) δ 3.13 (d, ^{3}J(P, H) = 10.75 Hz, 2H, CH_2), 3.27 (d, ^{3}J(P, H) = 7.55 Hz, 2H, CH_2), 4.76 (d, ^{2}J(P, H) = 12.55 Hz, 2H, $NH_{endocyclic}$), 7.28 (d, ^{3}J(H, H) = 8.8 Hz, 2H, Ar–H), 7.41 (d, ^{3}J(H, H) = 8.8 Hz, 2H, Ar–H), 7.62 (d, ^{2}J(P, H) = 5.6 Hz, 1H, NHP), 9.65 (s, 1H, 4-CN-C_6H_4NH). ^{13}C NMR (125.76 MHz, d_6-DMSO) δ 40.9 (d, ^{2}J(P, C) = 11.56 Hz), 119.66 (s), 125.52(s), 128.61(s), 138.29(s), 153.03(d, ^{2}J(P, C) = 2.6 Hz).^{31}P NMR (202.46 MHz, d_6-DMSO) δ 23.53 (m). IR (KBr, cm^{-1}): 3379(*v*N–H), 3140, 2918, 1706 (*v*C=O), 1592, 1525, 1485, 1413, 1365, 1297, 1217, 1157 (*v*P=O), 1106, 1054 (*v*P–N), 938, 772, 545, 488, 445.

2-(N-3-methyl-phenylureido)-1,3,2-diazaphospholane-2-oxide ***(29)*** Yield: 73 %, m.p. 195–196 °C. ^{1}H NMR (500.13 MHz, d_6-DMSO) δ 2.17 (s, 3H, CH_3), 3.12 (d, ^{3}J(P, H) = 12.0 Hz, 2H, CH_2), 3.23 (d, ^{3}J(P, H) = 7.95 Hz, 2H, CH_2), 4.8 (d, ^{2}J(P, H) = 12.45 Hz, 2H, $NH_{endocyclic}$), 6.89 (t, ^{3}J(H, H) = 7.25 Hz, 1H, Ar–H), 7.09 (d, ^{3}J(H, H) = 7.5 Hz, 1H, Ar–H), 7.11 (d, ^{3}J(H, H) = 7.65 Hz, 1H, Ar–H), 7.81 (s, 1H, PNH), 7.92 (d,^{3}J(H, H) = 8.1 Hz,1H, Ar–H), 9.38 (s, 1H, 3-CH_3-C_6H_4NH). ^{13}C NMR (125.76 MHz, d_6-DMSO) δ 17.73(s), 40.9 (d, ^{2}J(P, C) = 11.44 Hz), 119.94 (s), 122.3(s), 126.09(s), 126.49(s), 130.04(s), 137.48 (s), 153.24(d, ^{2}J(P, C) = 2.4 Hz).^{31}P NMR (202.46 MHz, d_6-DMSO) δ 24.1 (m). IR (KBr, cm^{-1}): 3368(*v*N–H), 2957, 2894, 1694(*v*C = O), 1614, 1591, 1540, 1481, 1455, 1411, 1295, 1210, 1168 (*v*P=O), 1109, 1050(*v*P–N), 944, 854, 824, 796, 749, 622, 571, 480.

2-(N-3-fluoro-phenylureido)-1,3,2-diazaphospholane-2-oxide ***(30)*** Yield: 75 %, m.p. 201–202 °C. ^{1}H NMR (500.13 MHz, d_6-DMSO) δ 3.09 (d, ^{3}J(P, H) = 10.11 Hz, 2H, CH_2), 3.18 (d, ^{3}J(P, H) = 5.4 Hz, 2H, CH_2), 4.76 (d, ^{2}J(P, H) = 12.6 Hz, 2H, $NH_{endocyclic}$), 6.76 (d, 1H, ^{3}J(H, H) = 4.28 Hz), 7.08 (t, ^{3}J(H, H) = 8. 9 Hz, 2H, Ar–H), 7.38 (dd, ^{3}J(H, H) = 8.9 Hz, ^{3}J(H, F) = 4.9 Hz, 1H, Ar–H), 7.56 (b, 1H, NHP), 9.54 (s, 1H, 3-F-C_6H_4NH). ^{13}C NMR (125.76 MHz, d_6-DMSO) δ 40.88 (d, ^{2}J(P, C) = 11.43 Hz), 115.16 (s), 115.46 (s), 119.8 (s), 119.9 (s), 153.13 (s). ^{31}P NMR (202.46 MHz, d_6-DMSO) δ 23.58 (m). IR (KBr, cm^{-1}): 3390(*v*N–H), 3250, 2955, 1701 (*v*C=O), 1612, 1546, 1509, 1484, 1405, 1292, 1217, 1153 (*v*P=O), 1101, 1055 (*v*P–N), 939, 825, 783, 747, 708, 460.

2-(N-3-nitro-phenylureido)-1,3,2-diazaphospholane-2-oxide ***(31)*** Yield: 55 %, m.p. 187-188 °C. ^{1}H NMR (500.13 MHz, d_6-DMSO) δ 3.17(d, ^{3}J(P, H) = 12.2 Hz, 2H, CH_2), 3.27 (d, ^{3}J(P, H) = 7.91 Hz, 2H, CH_2), 4.85 (d, ^{2}J(P, H) = 12.7 Hz, 2H, $NH_{endocyclic}$), 7.01 (t, ^{3}J(H, H) = 8.2 Hz, 1H, Ar–H), 7.22 (d, ^{3}J(H, H) = 7.9 Hz, 1H, Ar–H), 7.31 (d, ^{3}J(H, H) = 7.5 Hz, 1H, Ar–H), 7.52 (s, 1H, PNH), 7.75 (d, ^{3}J(H, H) = 8.0 Hz, 1H, Ar–H), 9.5 (s, 1H, 3-NO_2-C_6H_4NH). ^{13}C NMR (125.76 MHz, d_6-DMSO) δ 40.9 (d, ^{2}J(P, C) = 11.4 Hz), 123.55 (s), 123.75(s), 125.17(s), 134.1(s), 134.5(s), 138.3(s), 153.1(d, ^{2}J(P, C) = 2.35 Hz).^{31}P NMR (202.46 MHz, d_6-DMSO) δ 23.53 (m). IR (KBr, cm^{-1}): 3370(*v*N–H), 3135, 1700(*v*C=O), 1544, 1493, 1402, 1344, 1214 (*v*P=O), 1158, 1094, 1069, 905, 859, 836, 805, 732, 675, 610, 578, 547.

2-(N-2-methyl-phenylureido)-1,3,2-diazaphospholane-2-oxide ***(32)*** Yield: 73 %, m.p. 195-196 °C. ^{1}H NMR (500.13 MHz, d_6-DMSO) δ 2.15 (s, 3H, CH_3), 3.12 (d, ^{3}J(P, H) = 12.13 Hz, 2H, CH_2), 3.2 (d, ^{3}J(P, H) = 7.3 Hz, 2H, CH_2), 4.75 (d, ^{2}J(P, H) = 12.35 Hz, 2H, $NH_{endocyclic}$), 6.93 (t, ^{3}J(H, H) = 7.33 Hz, 1H, Ar–H), 7.1 (d, ^{3}J(H, H) = 7.5 Hz, 1H, Ar–H), 7.18 (d, ^{3}J(H, H) = 7.61 Hz, 1H, Ar–H), 7.31 (s, 1H, PNH), 7.52 (d,^{3}J(H, H) = 7.92 Hz,1H, Ar–H), 9.21 (s, 1H, 2-CH_3-C_6H_4NH). ^{13}C NMR (125.76 MHz, d_6-DMSO) δ 17.52(s), 40.92 (d, ^{2}J(P, C) = 11.31 Hz), 119.87 (s), 122.3(s), 126.1 (s), 126.53(s), 130.02(s), 137.26 (s), 153.24(d, ^{2}J(P, C) = 2.2 Hz).^{31}P NMR (202.46 MHz, d_6-DMSO) δ 24.12 (m). IR (KBr, cm^{-1}): 3375(*v*N–H), 3150, 2895, 1701 (*v*C=O), 1693, 1612, 1588, 1537, 1490, 1452, 1408, 1290, 1209, 1165 (*v*P=O), 1106, 1048 (*v*P–N), 941, 850, 745, 618, 568, 476.

2-(N-2-fluoro-phenylureido)-1,3,2-diazaphospholane-2-oxide ***(33)*** Yield: 70 %, m.p. 201–202 °C. ^{1}H NMR (500.13 MHz, d_6-DMSO) δ 3.12 (d, ^{3}J(P, H) = 12.88 Hz, 2H, CH_2), 3.26 (d, ^{3}J(P, H) = 9.89 Hz, 2H, CH_2), 4.76 (d, ^{2}J(P, H) = 12.61 Hz, 2H, $NH_{endocyclic}$), 6.81 (d, ^{2}J(H, H) = 4.43 Hz, 1H, Ar–H), 7.08 (t, ^{3}J(H, H) = 8.9 Hz, 2H, Ar–H), 7.39 (dd, ^{3}J(H, H) = 8.96 Hz, ^{3}J(H, F) = 4.9 Hz, 1H, Ar–H), 7.58 (s, 1H, NHP), 8.03 (b,1H, Ar–H), 9.54 (s, 1H, 2-F-C_6H_4NH). ^{13}C NMR (125.76 MHz, d_6-DMSO) δ

40.89 (d, ^2J(P, C) = 11.59 Hz), 114.94 (s), 115.16 (s), 115.45 (s), 119.86 (d, ^2J(F, C) = 7.8 Hz), 135.66 (d, ^2J(F, C) = 2.3 Hz), 153.16 (d, ^2J(P, C) = 2.7 Hz). ^{31}P NMR (202.46 MHz, d_6-DMSO) δ 23.66 (m). IR (KBr, cm^{-1}): 3390(νN–H), 3250, 2955, 1701 (νC=O), 1612, 1546, 1509, 1484, 1405, 1292, 1217, 1153 (νP=O), 1101, 1055 (νP–N), 939, 825, 783, 747, 708, 460.

2-(N-2-nitro-phenylureido)-1,3,2-diazaphospholane-2-oxide (***34***) Yield: 60 %, m.p. 187–188 °C. ^{1}H NMR (500.13 MHz, d_6-DMSO) δ 3.14(d, ^3J(P, H) = 12.6 Hz, 2H, CH_2), 3.25 (d, ^3J(P, H) = 8.9 Hz, 2H, CH_2), 4.7 (d, ^2J(P, H) = 12.7 Hz, 2H, $NH_{endocyclic}$), 7.2 (t, ^3J(H, H) = 7.9 Hz, 1H, Ar–H), 7.65 (t, ^3J(H, H) = 8.0 Hz, 1H, Ar–H), 8.02 (d, ^3J(H, H) = 8.15 Hz, 1H, Ar–H), 8.2 (d, ^3J(H, H) = 8.4 Hz, 1H, Ar–H), 8.39 (s, 1H, PNH), 10.3 (s, 1H, 2-NO_2-C_6H_4NH). ^{13}C NMR (125.76 MHz, d_6-DMSO) δ 40.9 (d, ^2J(P, C) = 11.52 Hz), 122.65 (s), 123.32(s), 125.12(s), 134.01(s), 134.5(s), 138.5(s), 153.06(d, ^2J(P, C) = 2.5 Hz, d).^{31}P NMR (202.46 MHz, d_6-DMSO) δ 22.94 (m). IR (KBr, cm^{-1}): 3334(νN–H), 3135, 2935, 1715(νC=O), 1609, 1586, 1483, 1433, 1344, 1278, 1209, 1172 (νP=O), 937, 864, 742.

Crystal structure determination

Crystals suitable for X-ray crystallography were obtained from ethanol at room temperature. X-ray data of compound **15** were collected on a Bruker SMART 1000 CCD (Bruker, 1998) area detector with graphite monochromated Mo Kα radiation (k = 0.71073 Å). The structure was refined with SHELXL-97 (Sheldrick, 2008) by full-matrix least-squares on F^2. The positions of hydrogen atoms were obtained from the difference Fourier map. An absorption correction was performed using the SADABS program for the titled structure.

Cytotoxicity assay

The cytotoxic activity of the synthesized compounds was determined on five human cancer cell lines: cervical cancer (HeLa), breast cancer (MCF-7 and MDA-MB-231), prostate cancer (PC-3), and leukemia (K562) by MTT assay. The cells suspended in the corresponding culture medium were inoculated in 96-well microtiter plates at a density of 2000–8000 cells per well and incubated for 24 h at 37 °C in a humidified atmosphere with 95 % air and 5 % CO_2. An equal volume of additional medium containing either the serial dilutions of the test compounds, positive control (cyclophosphamide), or negative control (2 %DMSO) was added to the desired final concentrations, and the microtiter plates were further incubated for 24, 48, and 72 h. Each assay was set up in triplicate wells and repeated one to three times. The IC_{50} value is defined as compound concentration that inhibits cell growth by 50 %. Also, to study the degree of selectivity in the cytotoxic activity of the compounds, separation of lymphocyte was down according to the following procedure (Bøyum, 1976): Defibrinated or anticoagulant-treated blood was diluted with an equal volume of PBS and layered carefully over Ficoll-Paque PLUS (without intermixing) in a centrifuge tube. After a short centrifugation at room temperature (typically at 400 g_{av} for 30–40 min), lymphocytes, together with monocytes and platelets, are harvested from the interface between the Ficoll-Paque PLUS and sample layers. This material was then centrifuged twice in a balanced salt solution to wash the lymphocytes and to remove the platelets.

Antibacterial evaluation assay

The cup-plate agar method (Barry, 1977) was used to determine the antibacterial activity of compounds **13–34** against three Gram-positive bacteria, namely *S. aureus* (ATCC 25923), *B. subtilis* (ATCC 12711), and *B. cereus* (ATCC 11778), three Gram-negative bacteria, viz. *E. coli* (ATCC 25922), *P. aeruginosa* (ATCC 27853), and *Proteus vulgaris* (NCIMB 8066). The compounds dissolved in dimethyl sulfoxide (DMSO) at a concentration of 6000 μg/cm^3 were used. Then, the solutions of the tested compounds were placed on the well of the media inoculated with the microorganisms. DMSO was used as a solvent control. Gentamicin and tetracycline were used as reference antibacterial drugs. The diameter of the growth inhibition zone was read after 24 h of incubation at 35 °C. These compounds were further examined by the broth dilution method to determine their MIC (minimal inhibitory concentration) (Vincent and Vincent, 1944). Minimal inhibitory concentrations were read after 24 h of incubation at 35 °C.

Computational details

The solid-state structures were used as the starting point for density functional theory (DFT) calculations in the gas phase and fully optimized at the B3LYP/6–31 + G* level. Whereas the X-ray crystallography cannot determine accurately the position of the H atoms, the optimization of H atom positions was performed to investigate the hydrogen bond characters in solid-state structures. To achieve this goal, the solid-state structure of a conformer was modeled as clusters in which the target molecule is surrounded by two neighboring conformers and a similar molecule (Fig. 5). The positions of H atoms were optimized for model clusters, while other atoms were kept frozen during the optimization. Such computational justifications have also been used to describe well the geometry

and electronic aspects of X-ray structures (Mirzaei *et al*., 2006; Esrafili *et al*., 2007). The NBO and AIM analyses have been performed to compare the electronic features of the gas-phase structures of the compound with those of model clusters at the B3LYP/6–311 + G** level. The hydrogen-bonding energies have been calculated on the basis of the energy difference between the hydrogen-bonded tetramer and its fragments, as represented in the equation $E_{HB}(1) = [E_{tetramer} - (E_{frag1} + E_{frag2})]/2$, where fragment 1 is composed of three monomers (conformers **A**, **B**, and **B′** on the left in Fig. 5) and fragment 2 is the right molecule (conformer **A′**). The $[E_{tetramer} - (E_{frag1} + E_{frag2})]$ term corresponds to the energies of the two symmetry-related contacts between the two pairs of molecules, and the value is therefore divided by 2. Also, other hydrogen-bonding energies have been calculated on the basis of the equation $E_{HB}(2)$, $(3) = [E_{tetramer} - (E_{frag1} + E_{frag2})]$, where fragment 1 is composed of three monomers (conformers **A**, **A′**, and **B** in $E_{HB}(2)$; conformers **A**, **A′**, and **B′** in $E_{HB}(3)$) and fragment 2 is the conformer **B′** in $E_{HB}(2)$ and conformer **B** in $E_{HB}(3)$, respectively. The hydrogen-bonding energies were then corrected for basis set superposition error (BSSE) using the counterpoise method (Boys and Bernardi, 1970). All quantum chemical calculations have been carried out using the *GAUSSIAN 03* package (Frisch *et al*., 2003) on a Pentium 4 (2.8 GHz CPU and 1024 MB RAM) work station.

Statistical analysis

In order to identify the effect of descriptors on the molecule's anticancer activity, QSAR studies were performed using the model described (Hansch and Fujita, 1964). The stepwise multiple linear regression (MLR) procedure, which is a common method used in QSAR studies, was used for selection of the descriptors using SPSS 16.0. The electronic and structural descriptors were obtained by both the quantum chemical calculations. The electronic descriptors included the highest occupied and lowest unoccupied molecular orbital (E_{HOMO} and E_{LUMO}), after highest occupied and next lowest unoccupied molecular orbital (E_{H-1} and E_{L+1}), the energy difference between the LUMO and HOMO (ΔE_{L-H}), electrophilicity (w) (Parr *et al*., 1999), polarizability (PL), and the net atomic charges (Q). Hydrophobic coefficient (log P), dipole moment (μ), molecular volume (Mv), and molecular total energy (TE) were the structural descriptors. E_H, E_L, E_{H-1}, E_{L+1}, w, PL, Q, μ, Mv, and TE (low optimized energy) values were obtained from the DFT results (Sharma *et al*., 2012). The logarithm of partition coefficient (log P) was calculated by the Viswanadhan's fragmentation method (Viswanadhan, 1989). In this study, only the variables that contain the necessary information for modeling were used. The principal component analysis (PCA) was utilized to find the relationship between the dependent and independent variables, reducing the set of independent variables (Pinto *et al*., 2001). The toxicities of 22 compounds, **CP**, and phenylurea were expressed in terms of IC_{50}, which is defined as necessary molar concentration of compound causing 50 % inhibition against human cell lines. All obtained IC_{50} values are usually converted into the negative logarithm of IC_{50} in QSAR study (log $(1/IC_{50})$).

Results and discussion

Spectroscopic study

Sixteen new derivatives of diazaphosphore with the general formula $RC_6H_4NHC(O)NHP(O)R^1R^2$ were synthesized (Scheme 1) (Kirsanov, 1954; Kirsanov and Zhmurova, 1956) and characterized by ^{31}P, ^{13}C, and ^1H NMR and IR spectroscopy. Comparison of the $\delta(^{31}P)$ data in Table 1 shows that chemical shift of compounds bearing nitro group is at the most upfield region rather than those of other groups (CH_3, F, and CN). For instance, derivative **32** (2-CH_3) shows ^{31}P chemical shift value 24.12 ppm, whereas derivatives **33** (2-F) and **34** (2-NO_2) exhibit 23.66 and 22.94 ppm, respectively. The ^{31}P NMR spectra of compounds **13–34** also show a chemical shift in the range from 2.86 (in **23**) to 24.12 (in **19**) ppm. ^{31}P nuclei in compounds **13–23** are shielded relative to those of other compounds. Inspection of ^1H and ^{13}C NMR spectra of the new derivatives **15**, **17–19**, and **22** reveals two separate signals for H_{axial} and $H_{equatorial}$ and carbons of two methyl groups. Also, it is observed from Table 1 two different signals of H_{axial} and $H_{equatorial}$ for compounds **24–33**. The $^3J(PNCH)$ coupling constant from 10.11 to 12.88 is related to the $H_{equatorial}$ atom, and for H_{axial} atom, the coupling with phosphorus atom is from 5.4 to 9.89 ppm. This led us to conclude that the synthesized compounds are toward one chair conformation (Denmark *et al*., 1999) that adopt with X-ray crystallography for **15**. The small values of $^3J(H, P)$ indicate that the relevant dihedral angles are close to orthogonal. In the case of compound **15**, the torsional angles of P–N–C–H_{axial} and P–N–C–$H_{equatorial}$ are ±68 and ±173, respectively, obtained from X-ray crystallography. Considering the Karplus equation (Breitmaier and Voelter, 1990), the $H_{equatorial}$ proton has the largest coupling with phosphorus atom. In these heterocycles, the highest value coupling constant is 24.76 and 12.88 Hz for diazaphosphorinane **20** and diazaphospholane **33**. In addition to the $\delta(^{31}P)$, $^2J(PNH)_{endocyclic}$ and $^2J(P,C)_{endocyclic}$ values in compounds **24–34** are larger than those of compounds **13–23**. The ^1H NMR spectrum of **24–34** exhibits a doublet signal for the two equivalent amino protons (of the five-

Scheme 1 Preparation pathway for the synthesis of compounds **13–34**

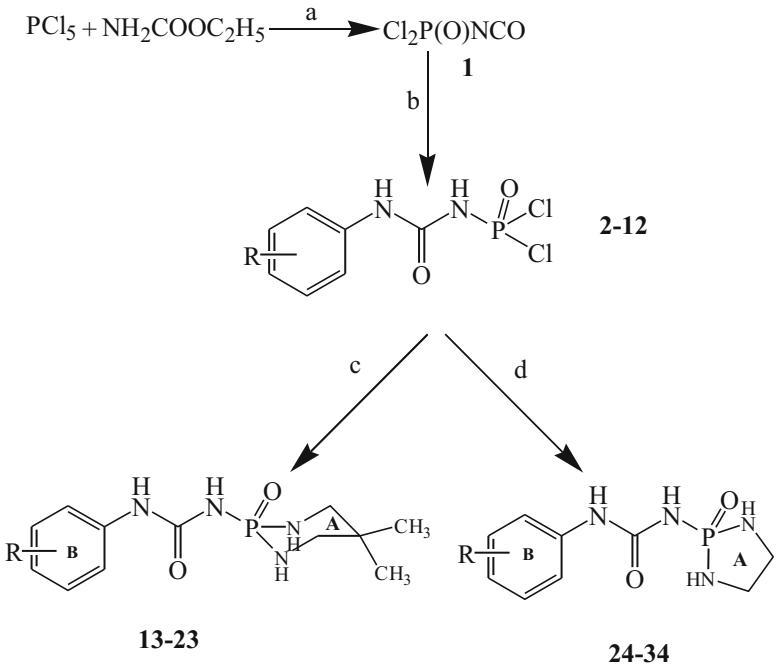

Reagents and conditions:
(a) 1,2-dicholoroethan
(b) Anilin derivatives, 0 ^{0}C
(c) 2,2-dimethyl-1,3-diaminopropane, 0 ^{0}C, diethyl ether
(d) ethylendiamine, triethylamine, 0 ^{0}C, dicholoromethane

Comp.	A-ring	B-ring	Comp.	A-ring	B-ring
13	diazaphosphorinane	4-H[i]	**24**	diazaphospholane	4-H
14	diazaphosphorinane	4-CH_3[ii]	**25**	diazaphospholane	4-CH_3
15	diazaphosphorinane	4-F	**26**	diazaphospholane	4-F
16	diazaphosphorinane	4-NO_2[i]	**27**	diazaphospholane	4-NO_2
17	diazaphosphorinane	4-CN	**28**	diazaphospholane	4-CN
18	diazaphosphorinane	3-CH_3	**29**	diazaphospholane	3-CH_3
19	diazaphosphorinane	3-F	**30**	diazaphospholane	3-F
20	diazaphosphorinane	3-NO_2[iii]	**31**	diazaphospholane	3-NO_2
21	diazaphosphorinane	2-CH_3[iii]	**32**	diazaphospholane	2-CH_3
22	diazaphosphorinane	2-F	**33**	diazaphospholane	2-F
23	diazaphosphorinane	2-NO_2[iii]	**34**	diazaphospholane	2-NO_2

For compounds **13**, **14**, **16**, **20**, **21**, and **23** see the following references: [i]Gholivand and Dorosti., 2011; [ii]Gholivand et al., 2012; [iii]Gholivand et al., 2010.

membered ring) with a high value for phosphorus–hydrogen coupling constant about 12.8 Hz and a doublet signal with ^{2}J(PNH) about 6.0 Hz for the amidic proton. ^{2}J(PNH) coupling constants of endocyclic amino protons in compounds containing six-membered (**13–34**) are in the range 2.5–3.8 Hz. The major reduction in the ^{2}J(PNH) coupling constant from 12.8 (in **27**) to 3.8 (in **15**) is due to the increase in ring size because the five-membered ring has high ring strain. Similar to the ^{2}J(PNH) value, ^{2}J(P, C)$_{endocyclic}$ was observed for diazaphospholanes **24–34** (about

Table 1 Spectroscopic data of compounds **13–34**

Comp.	δ^{31}P (ppm)	^{2}J(P,H)$_{exo}$ (HZ)	^{2}J(P,H)$_{endo}$ (HZ)	^{3}J(PNCH) (HZ)	^{2}J(P,C)$_{exo}$ (HZ)	^{2}J(P,C)$_{endo}$ (HZ)	^{3}J(P,C)$_{endo}$ (HZ)	$\nu_{P=O}$	$\nu_{C=O}$
13[a]	3.78	6.76	2.7	24.2	2.3	1.76	4.3	1170	1677
14[b]	3.85	7.15	3.5	24.1	–		4.1	1180	1686
15	3.72	–	3.8	24.4	2.38	1.4	4.2	1178	1690
16[a]	3.23	7.59	–	24.3	–		4.53	1196	1699
17	3.6	3.65	2.5	24.36	1.94	–	4.33	1187	1709
18	4.62	–	–	m	2.54	–	3.5	1193	1680
19	3.8	5.18	–	m	2.49	4.5	–	1178	1690
20[c]	3.41	–	3.4	24.76	2.54	1.42	4.33	1176	1699
21[c]	4.62	–	–	21.9	–	–	3.5	1190	1680
22	3.79	7.1	3.28	m	2.57	–	4.5	1178	1690
23[c]	2.86	–		23.1	–		4.62	1164	1702
24	23.54	0.0	12.5	12.85(eq), 7.1(ax)	2.3	11.52	–	1155	1695
25	23.65	6.0	12.35	12.65(eq), 7.4(ax)	2.45	11.53	–	1159	1694
26	23.58	0.0	12.30	12.0(eq), 7.8(ax)	1.89	11.55	–	1153	1701
27	23.30	0.0	12.8	12.85(eq), 7.65(ax)	2.64	11.78	–	1155	1705
28	23.53	5.6	12.55	10.75(eq), 7.55(ax)	2.6	11.56	–	1157	1706
29	24.1	0.0	12.45	12.0(eq), 7.95(ax)	2.4	11.44	–	1168	1694
30	23.58	–	12.6	10.11(eq), 5.4(ax)	–	11.43	–	1153	1701
31	23.53	–	12.7	12.2(eq), 7.91(ax)	2.35	11.4	–	1165	1701
32	24.12	–	12.35	12.13(eq), 7.3(ax)	2.2	11.31	–	1156	1701
33	23.66	0.0	12.6	12.88(eq), 9.89(ax)	2.7	11.59	–	1153	1701
34	22.94	0.0	12.7	12.6(eq), 8.9(ax)	2.5	11.52	–	1172	1715

For compounds **13**, **14**, **16**, **20**, **21**, and **23**, see the following references: [a]Gholivand and Dorosti, 2011; [b]Gholivand *et al*., 2012; [c]Gholivand *et al*., 2010

11.51 Hz), which are larger than the values of diazaphosphorinanes **13–23**. ^{3}J(P, C) coupling constant was obtained for compounds **13–24** (3.5–4.62 Hz).

X-ray crystallography

Single crystals of compound **15** were obtained by slow evaporation of the solvent at room temperature. Compound crystallizes in the monoclinic crystal system with space group $P2_1/n$, and the crystal system contains two independent molecules (**15a** and **15b**). The crystallographic data, bond lengths, and angles are listed in Tables 2 and 3, respectively. Molecular structures are shown in Fig. 2. The molecules are significantly different as manifested by their torsion angles. For instance, the O1P1N1C1, O1AP1AN1AC1A, and O1P1N2C3, O1AP1AN2AC3A torsion angles are −162.26°, 160.29° and 165.49°, −164.53°, respectively. The P=O distances in molecules **15a** and **15b** are 1.4818 and 1.4823 Å and are larger than the normal P=O bond length (1.45 Å) (Corbridge 1995). These values are comparable to those reported for phosphoramidates (Gholivand and Dorosti 2011; Gholivand *et al*. 2009). The P atoms have slightly distorted tetrahedral configurations with the surrounding angles around the P atoms in the range of 101.92 (9)°–116.36 (10)° and 101.84 (9)°–116.14 (9)° for molecules **15a** and **15b**, respectively. The P–N $_{endocyclic}$ distances are significantly shorter than the related P–$N_{C(O)NHP(O)}$ bond distance (Table 3). All of these bonds are in the range 1.6218(18)–1.6985(18) Å and thus are significantly shorter than a typical P–N single bond (1.77 Å) (Roy *et al*., 2006). The P=O bonds in molecules **15a** and **15b** are in an equatorial position of the related 1, 3-diazaphosphorinane rings. The endocyclic nitrogen atoms in compounds **15a** and **15b** are distorted from planarity. The sum of angles around these atoms in **15a** is 353.15° and 353.69° for N(1) and N(2) atoms, and in **15b**, is 351.39° and 352.72° for N(7) and N(8) atoms. The sum of the surrounding angles for all the exocyclic nitrogen atoms is almost 360°; therefore, the environment of the N atoms is practically planar. As shown in Fig. 3, the carboxyl and phosphoryl groups of ligands are involved in intermolecular N–H…O hydrogen bonding and form two types of robust hydrogen bond synthons, namely R_2^2 (8) **I** and R_6^6(28) **II**. These intermolecular interactions connected the various components into a 2D network. There are also intramolecular P = O…H-NPh hydrogen bonds in

Table 2 Crystallographic data for compound **15**

Compound	**15**
Empirical formula	$C_{12}H_{18}F\ N_4O_2P$
Formula weight	300.27
Temperature	120(2) K
Wavelength	0.71073 Å
Crystal system	Monoclinic
Space group	P 21/n
Unit cell dimensions	$a = 17.3891(16)$ Å $\alpha = 90°$
	$b = 5.7264(5)$ Å $\beta = 9.635(2)°$
	$c = 28.892(3)$ Å $\gamma = 90°$
Volume	2836.4(4) $Å^3$
Z	8
Density (calculated)	1.406 Mg/m^3
Absorption coefficient	0.213 mm^{-1}
$F(000)$	1264
Crystal size	0.30 × 0.30 × 0.05 mm^3
Theta range for data collection	1.43–28.99°
Index ranges	$-23 \le h \le 23$, $-7 \le k \le 7$, $-39 \le l \le 39$
Reflections collected	26921
Independent reflections	7536 [R(int) = 0.0557]
Completeness to theta = 28.99°	99.9 %
Absorption correction	Semi-empirical from equivalents
Max. and min. transmission	0.984 and 0.939
Refinement method	Full-matrix least-squares on F^2
Data/restraints/parameters	7536/0/365
Goodness of fit on F^2	1.001
Final R indices	$R_1 = 0.0483$, w$R_2 = 0.1073$
R indices (all data)	$R_1 = 0.0896$, w$R_2 = 0.1208$
Largest diff. peak and hole	0.781 and −0.430 e $Å^{-3}$

both conformers. In addition to numerous strong hydrogen bonds, intermolecular interactions in **15** include weaker C9A-H9AA…F1A^{i} ($i = 1/2 - x, -1/2 + y, -1/2 - z$) interaction with C…F distance of 3.146(2). There are also C–H…π interactions [H… centroid distance = 2.82 (2), 2.72(2) Å] that occur between C1-H1B, C11AH11B, and Cg2 [Cg2^{i} ($i = -x, 2 - y, -z$), Cg2^{ii} ($ii = x, y, z$)] as well as [H… centroid distance = 2.96 (2), 2.96 (2) Å] that occur between C1A–H1AA, C11H11A, and Cg4 [Cg4^{i} ($i = 1 - x, 1 - y, -z$), Cg4^{ii} ($ii = x, 1 + y, z$)].

Cytotoxic activity

The goal of this study was to gain further insights into the structural requirements for the anticancer activity of diazaphosphore derivatives. Hence, the in vitro antitumor activities of the 22 synthesized compounds, namely diazaphosphorinane (**13**–**23**) and diazaphospholane (**24**–**34**) with –NHC(O)NHP(O)– functional group, were evaluated by MTT assay against five human cancer cell lines: cervical cancer (HeLa), breast cancer (MCF-7 and MDA-MB-231), prostate cancer (PC-3), and leukemia (K562), with cyclophosphamide (**CP**) as the positive control. Their IC_{50} values are listed in Table 4. The plots of IC_{50} values for all of the compounds are also shown in Fig. 4. As shown in Table 4, most of the compounds displayed higher activity than phenyl urea against the selected cell lines and even preferable cytotoxic activities than the commercial anticancer drug **CP** with slightly different capacity, which was consistent with our previous studies (Gholivand *et al*., 2010, 2012). On the basis of our previous work, –N^{1}HC(O)N^{2}HP(O)– scaffold was assayed as the optimum structure and the side chain of at *P*-position would be the key moiety to be explored. Thus, we attempted to replace the substituent on the phenyl ring attached to N^{1}H group with electron-donating and electron-withdrawing groups which are usually considered to play a key role in cytotoxic

Table 3 Optimized and experimental geometries of compound **15**

Parameters	Experimental	B3LYP/6-31 + G*	B3LYP/6-311 + G**
Bond lengths (Å)			
P(1)–N(2)	1.6218 (18)	1.671	1.666
P(1)–N(1)	1.6315 (18)	1.670	1.665
P(1)–N(3)	1.6985(18)	1.719	1.715
P(1A)–N(2A)	1.6268 (18)	1.671	1.665
P(1A)–N(1A)	1.6299 (17)	1.670	1.665
P(1A)–N(3A)	1.6948 (18)	1.719	1.715
Bond angles (°)			
O(1)–P(1)–N(2)	113.71 (9)	114.292	114.292
O(1)–P(1)–N(1)	116.36 (10)	117.282	117.372
O(1)–P(1)–N(3)	107.89 (9)	107.740	107.621
O(1A)–P(1A)–N(2A)	113.87 (9)	114.291	114.290
O(1A)–P(1A)–N(1A)	116.14 (9)	117.287	117.378
O(1A)–P(1A)–N(3A)	107.81 (9)	107.740	107.621
Torsion angles			
O(1)–P(1)–N(1)–C(1)	−162.26 (14)	−159.366	−157.488
O(1)–P(1)–N(2)–C(3)	165.49 (15)	163.487	161.872
N(3)–P(1)–N(1)–C(1)	77.93 (17)	80.139	82.134
N(3)–P(1)–N(2)–C(3)	−72.80 (18)	−74.409	−76.214
O(1A)–P(1A)–N(1A)–C(1A)	160.29 (15)	159.375	157.467
O(1A)–P(1A)–N(2A)–C(3A)	−164.53 (15)	−163.499	−161.859
N(3A)–P(1A)–N(1A)–C(1A)	−80.00 (17)	−80.128	−82.155
N(3A)–P(1A)–N(2A)–C(3A)	73.73 (17)	74.397	76.228

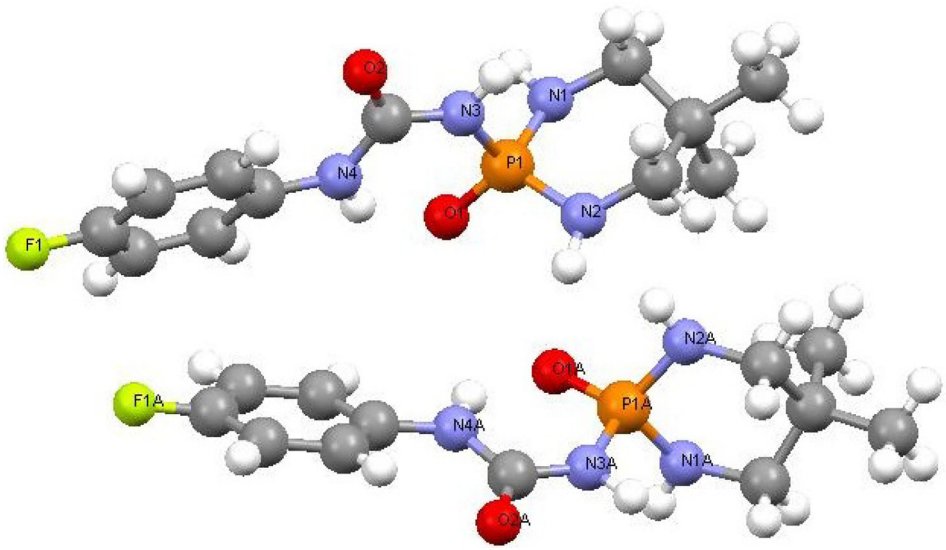

Fig. 2 Molecular structure of **15** with its atom (50 % probability level) labeling scheme

via drug–target interactions. When H unit was replaced with methyl, fluoro, and nitro substituent, data showed that electron-donating substituents revealed better activities than electron-withdrawing substituents such as **18** (3-CH_3, IC_{50}, 1.33 μM), **19** (3-F, IC_{50}, 4.75 μM), and **20** (3-NO_2, IC_{50}, 8.58 μM) against MCF-7 cells. Similarly, **18** (3-CH_3, IC_{50}, 2.25 μM), **21** (2-CH_3, IC_{50}, 2.66 μM), and **29** (3-CH_3, IC_{50}, 0.88 μM) exhibited higher activities than the other substituents such as **16** (4-NO_2, IC_{50}, 6.70 μM), **26** (4-F, IC_{50}, 5.41 μM), and **31** (3-CN, IC_{50}, 8.97 μM)

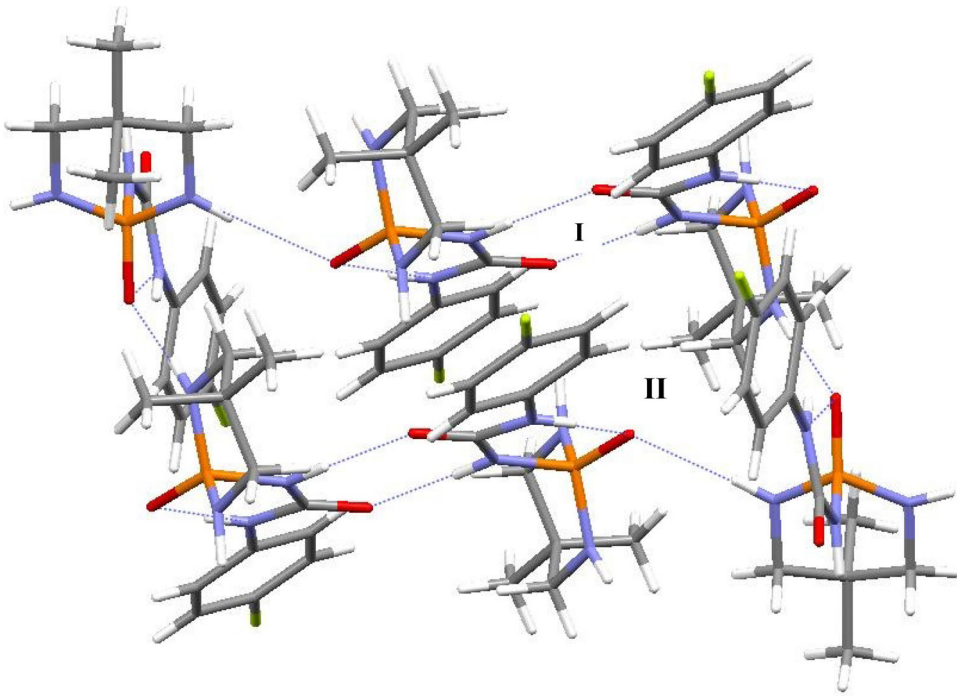

Fig. 3 A view of the robust N–H…O hydrogen bond synthons, $R_2^2(8)$ **I** and $R_6^6(28)$ **II**, that link the molecules forming a two-dimensional network in **15** (the *dashed lines* show donor–acceptor distances of hydrogen bonds)

against MDA-MB-231 cells. For this reason, synthesis of methyl analogs of this class compounds seems to be beneficial for anticancer drug design. Likewise, the above-mentioned structure–activity relationship was also found in the other titled cell lines. It is noteworthy that replacement of H with the selected groups at 4-position of aromatic ring did not follow a clear trend against the studied cell lines. In an attempt to explore the effects of substituent insertion in different positions of phenyl ring on the activity, the H in aromatic ring was replaced with 4-, 3-, and 2-methyl, fluorine, and nitro to afford the corresponding compounds (**14**–**16**, **25**–**27**), (**18**–**20**, **29**–**31**), and (**21**–**23**, **32**–**34**), respectively. Table 4 demonstrates that the newly synthesized methyl analogs exhibited antitumor activity on the studied cell lines with the average activity order of 3-CH_3 > 2-CH_3 > 4-CH_3 such as **29** (3-CH_3, IC_{50}, 1.74 μM), **32** (2-CH_3, IC_{50}, 6.08 μM), and **25** (4-CH_3, IC_{50}, 13.90 μM) against PC-3 cells, whereas cell lines from our panel respond to nitro and fluoro analogs significantly differently. Finally, replacement of the six-membered ring in **13**–**23** with a five-membered ring **24**–**34** resulted in an interesting structure–activity correlation in two carcinoma cells, HeLa and MCF-7. For instance, fluorine analogs (**15**; 4-F, IC_{50}, 3.94 μM, **19**; 3-F, IC_{50}, 4.75 μM, and **22**; 2-F, IC_{50}, 3.14 μM) in six-membered ring displayed slightly higher average potency in comparison with these analogs in five-membered ring (**26**; 4-F, IC_{50}, 16.64 μM, **30**; 3-F, IC_{50}, 16.06 μM, and **33**; 2-F, IC_{50}, 3.2 μM) against MCF-7. Also, among modified analogs, *ortho* substituent in diazaphosphorinane ring (**21**; 2-CH_3, 2.13 μM, **22**; 2-F, 3.14 μM, **23**; 2-NO_2, 5.64 μM) showed higher anticancer activity than similar counterpart in diazaphospholane ring (**32**; 2-CH_3, 6.69 μM, **33**; 2-F, 3.2 μM, **34**; 2-NO_2, 17.57 μM) against MCF-7, suggesting that the ring size plays a significant role for activity. It can be explained by reduction of the electron donation to the phosphorus atom in five-membered ring compared to six-membered ring. In contrast, as shown in Table 1, inhibitory activities of *meta* and *para* positions to the titled cancer cell lines were different. For example, phosphorinane derivatives **16** (4-NO_2) and **18** (3-CH_3) showed an IC_{50} value 8.92 and 1.33 μM against MCF-7 cell line, whereas phospholanes **27** (4-NO_2) and **29** (3-CH_3) exhibited IC_{50} values of 1.28 and 0.72 μM, respectively. These differences may result from a number of factors, in addition to the interaction with the target involved in the cytostatic/cytotoxic response. These factors include number of cell cycles during the incubation period, drug uptake, efflux, and metabolism. On the other hand, few differences among cell lines would suggest that some non-specific cytotoxic effects are responsible for the activity of the tested compounds. To study the degree of selectivity in the cytotoxic activity of the compounds, assays using lymphocyte isolation from whole human blood were carried out on some representative compounds such as **14**, **20**, and **33**, which showed relatively high activity in tumor cells. The assay showed that survival values were 97 % for these compounds.

Antibacterial activity

The in vitro antibacterial activity of the synthesized derivatives **13**–**34** was tested against three Gram-positive

Table 4 In vitro antiproliferative activity of derivatives **13–34**, cyclophosphamide (**CP**), and phenylurea

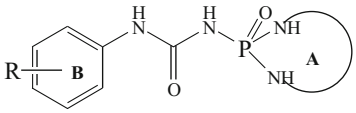

Compound	A-ring	B-ring	IC_{50}^{a}(μM) ± SD				
			HeLa	MCF-7	K562	PC-3	MDA-MB-231
13	Diazaphosphorinane	4-H	3.33 ± 0.35	6.2 ± 0.71	4.75 ± 0.15	29.66 ± 2.41	4.13 ± 0.24
14	Diazaphosphorinane	4-CH_3	6.51 ± 0.92	2.32 ± 0.03	4.14 ± 0.27	5.06 ± 0.11	2.96 ± 0.09
15	Diazaphosphorinane	4-F	3.05 ± 0.19	3.94 ± 0.27	8.17 ± 0.65	3.45 ± 0.32	5.29 ± 0.28
16	Diazaphosphorinane	4-NO_2	–	8.92 ± 0.58	7.23 ± 0.39	2.82 ± 0.18	6.70 ± 0.91
17	Diazaphosphorinane	4-CN	4.80 ± 0.82	5.52 ± 0.97	11.46 ± 1.70	2.68 ± 0.31	0.49 ± 0.05
18	Diazaphosphorinane	3-CH_3	1.52 ± 0.06	1.33 ± 0.10	1.64 ± 0.02	1.10 ± 0.27	2.25 ± 0.72
19	Diazaphosphorinane	3-F	3.50 ± 0.42	4.75 ± 0.64	9.75 ± 1.85	7.31 ± 0.49	3.03 ± 0.74
20	Diazaphosphorinane	3-NO_2	5.56 ± 0.21	8.58 ± 1.51	–	3.89 ± 0.23	5.25 ± 0.25
21	Diazaphosphorinane	2-CH_3	2.10 ± 0.36	2.13 ± 0.77	3.84 ± 0.63	2.24 ± 0.17	2.66 ± 0.83
22	Diazaphosphorinane	2-F	17.70 ± 2.89	3.14 ± 0.67	4.50 ± 0.73	4.01 ± 0.12	4.77 ± 0.33
23	Diazaphosphorinane	2-NO_2	3.32 ± 0.01	5.64 ± 0.22	2.82 ± 0.07	3.95 ± 0.44	4.69 ± 0.06
24	Diazaphospholane	4-H	6.42 ± 0.13	8.10 ± 0.55	–	30.08 ± 3.51	0.68 ± 0.03
25	Diazaphospholane	4-CH_3	–	9.67 ± 0.39	–	13.95 ± 2.98	5.59 ± 0.20
26	Diazaphospholane	4-F	4.25 ± 0.26	16.64 ± 1.34	4.67 ± 0.27	18.38 ± 3.52	5.41 ± 0.53
27	Diazaphospholane	4-NO_2	2.90 ± 0.79	1.28 ± 0.25	–	2.59 ± 0.55	2.01 ± 0.04
28	Diazaphospholane	4-CN	3.07 ± 0.06	1.69 ± 0.99	–	1.69 ± 0. 29	2.84 ± 0.38
29	Diazaphospholane	3-CH_3	1.35 ± 0.31	0.72 ± 0.02	3.00 ± 0.16	1.74 ± 0.27	0.88 ± 0.07
30	Diazaphospholane	3-F	–	16.06 ± 2.91	5.82 ± 0.59	4.09 ± 0.89	–
31	Diazaphospholane	3-NO_2	30.02 ± 4.37	5.75 ± 0.38	–	6.54 ± 0.41	8.97 ± 0.11
32	Diazaphospholane	2-CH_3	5.38 ± 0.44	6.69 ± 0.71	4.05 ± 0.22	6.08 ± 0.39	1.40 ± 0.01
33	Diazaphospholane	2-F	–	3.20 ± 0.03	–	–	1.65 ± 0.16
34	Diazaphospholane	2-NO_2	–	17.57 ± 3.00	20.65 ± 3.80	4.44 ± 0.39	8.94 ± 0.88
35	Phenyl urea[a]		10.22 ± 0.48	7.79 ± 0.92	16.07 ± 1.06	15.07 ± 2.21	17.6 ± 2.31
36	Cyclophosphamide[a]		7.09 ± 0.29	39.64 ± 3.94	41.23 ± 5.31	13.39 ± 2.91	2.70 ± 0.33

[a] IC_{50} is in terms of mM

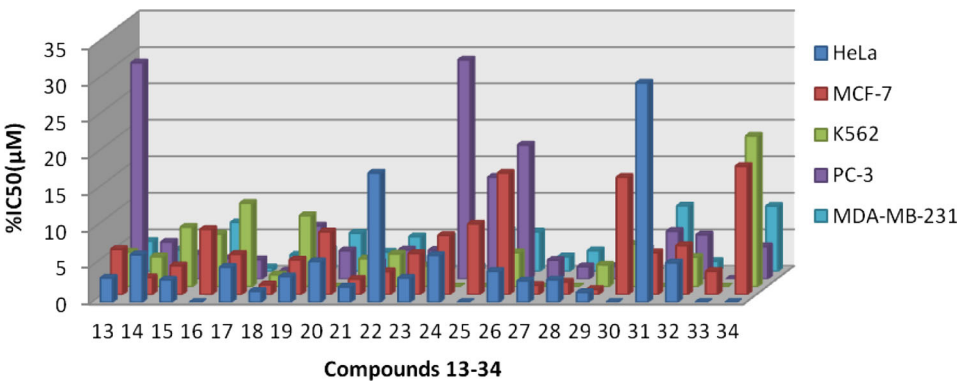

Fig. 4 IC_{50} values of compounds **13–34** against HeLa, MCF-7, K562, PC-3, and MDA-MB-231

Table 5 Diameter of inhibition zone and MIC values[a] of compounds **13–34** against selected microorganisms

Com.	A-ring	B-ring	Gram-positive bacteria						Gram-negative bacteria					
			S. aureus		*B. cereus*		*B. subtilis*		*E. coli*		*P. aeruginosa*		*P. vulgaris*	
			Z[a]	MIC[a]	Z	MIC	Z	MIC	Z	MIC	Z	MIC	Z	MIC
13	Diazaphosphorinane	4-H	12	385	–	–	6	>2500	11	1000	7	>2500	–	–
14	Diazaphosphorinane	4-CH_3	11	1000	7	>2500	11	500	10	1000	20	>2500	–	–
15	Diazaphosphorinane	4-F	10	>2500	16	>2500	17	>2500	–	–	–	–	–	–
16	Diazaphosphorinane	4-NO_2	11	600	6	1200	14	300	11	1200	11	1200	–	–
17	Diazaphosphorinane	4-CN	12	>2500	8	>2500	17	>2500	–	–	–	–	–	–
18	Diazaphosphorinane	3-CH_3	10	1200	–	–	12	600	–	–	–	–	–	–
19	Diazaphosphorinane	3-F	11	>2500	–	–	16	833	–	–	–	–	–	–
20	Diazaphosphorinane	3-NO_2	–	–	9	>2500	18	>2500	–	–	–	–	–	–
21	Diazaphosphorinane	2-CH_3	10	>2500	–	–	11	>2500	–	–	–	–	–	–
22	Diazaphosphorinane	2-F	9	>2500	–	–	15	25	–	–	–	–	–	–
23	Diazaphosphorinane	2-NO_2	–	–	11	>2500	–	–	–	–	–	–	–	–
24	Diazaphospholane	4-H	–	–	–	–	–	–	–	–	–	–	–	–
25	Diazaphospholane	4-CH_3	–	–	–	–	–	–	–	–	–	–	–	–
26	Diazaphospholane	4-F	–	–	–	–	–	–	–	–	–	–	–	–
27	Diazaphospholane	4-NO_2	–	–	–	–	–	–	–	–	–	–	–	–
28	Diazaphospholane	4-CN	–	–	–	–	–	–	–	–	–	–	–	–
29	Diazaphospholane	3-CH_3	–	–	–	–	8	>2000	–	–	–	–	–	–
30	Diazaphospholane	3-F	–	–	7	>2500	12	>1000	–	–	–	–	–	–
31	Diazaphospholane	3-NO_2	8	>2500	8	>2500	10	>2500	–	–	–	–	–	–
32	Diazaphospholane	2-CH_3	10	>2500	–	–	7	>2500	–	–	–	–	–	–
33	Diazaphospholane	2-F	9	>2500	8	>2500	13	>2000	–	–	–	–	–	–
34	Diazaphospholane	2-NO_2	8	>1000	–	–	–	–	–	–	–	–	–	–
Gentamicin			23	>500	27	125	33	125	26	125	25	125	22	125
Tetracycline			33	0.025	40	>0.025	36	>0.025	33	>0.025	31	>0.05	25	0.025

[a] The values indicate the diameters in mm for the zone of growth inhibition (GIZ) and minimal inhibitory concentration (MIC) in μg/ml observed after 24 h of incubation at 35 °C. Error values are within ±1 mm. Moderately active (8–13); highly active (>14)

–, not active

bacteria, viz. *S. aureus* (ATCC 25923), *B. subtilis* (ATCC 12711), and *B. cereus* (ATCC 11778), and three Gram-negative bacteria, viz. *E. coli* (ATCC 25922), *P. aeruginosa* (ATCC 27853), and *Proteus vulgaris* (NCIMB 8066), using the cup test method and minimum inhibitory concentration (MIC) experiments. While carrying out antibacterial activity, gentamicin and tetracycline were used as reference compounds and MIC were determined in terms of μg/ml (Table 5). Twenty-two heterocyclic compounds with six- and five-membered rings of phosphor were prepared and evaluated. At first, the objective was to identify the effect of A-ring size on activity. A perusal of the results from Table 5 reveals that diazaphosphorinanes (**13–23**) with six rings showed higher activity toward the tested Gram-positive bacteria than diazaphospholane (**24–34**) with five rings. For example, **19** with six rings (3-F, MIC; 833 μg/ml) exhibited potent activity against *B. subtilis* than **30** with similar structure attached to five rings (3-F, MIC; > 1000 μg/ml). The second goal was to identify substitution effect on activity against the selected microorganisms. Among the synthesized analogs at *para* position, the most potent compound against *S. aureus* and *B. subtilis* was **16**. It has NO_2 group attached, whereas when CH_3, F, and CN group substituents were attached to ring, the same as in case of **17** (4-CN), inhibition decreased (Table 5). Further, if NO_2 group is attached to *meta* and *ortho* positions, activity decreased as observed in **20** and **23**, respectively. Reduced activity was observed when CH_3 group was attached at the titled positions as in compounds **18** and **21**, whereas substitution of (3-F, 2-F) group to the phenyl group of **19** and **22** compounds increased inhibitory activity against *B. subtilis*. The most valuable finding is the inhibition of *B. subtilis* growth by compound **22** (MIC, 25 μg/ml) having electron-withdrawing group (F) at *ortho* position. The MIC values of compounds against certain bacterial strains indicate that *B. subtilis* were more

sensitive to the toxicity of the synthesized compounds than other microorganisms. In addition, only derivatives **13**, **14**, and **16** showed negligible activities against *E. coli* and *P. aeruginosa* as compared to reference drugs.

NBO and AIM analyses

Fully optimized conformers in the gas phase

The geometries of conformers **15a** and **15b** were separately optimized as single molecules in vacuum in order to compare the structural and energy aspects of the two conformers in the gas phase. The optimized geometries were confirmed to be the minimum energy point with no imaginary vibrations. The P=O, P–N, C–N, and N–H bond lengths, charge densities, and vibrational data have been represented in Table S1 for two conformers. In both of the conformers, the weak intramolecular CH…OC hydrogen bond between the *ortho*-proton of the 4-FC_6H_4NH and the carbonyl O atom creates a six-membered ring via the O–C–N–C–C–H bond paths. This intramolecular contact stabilizes a *gauche* configuration between the C=O bond and the *ortho*-proton of 4-fluoroaniline. Furthermore, intramolecular 4-FC_6H_4N-H…O=P hydrogen bond creates a six-membered ring via the O–P–N–C–N–H bond paths. Based on the results of DFT calculations, we found that the change in basis set used for geometry optimizations has no significant effect on the measure of structural parameters and the two optimized conformers convert to a unique structure. Hence, only one molecular structure was selected to obtain electronic properties by AIM and NBO analyses. The NBO analysis reveals a weak electronic delocalization between the lone pair of the carbonyl oxygen, Lp(OC), and the vacant σ^*(C-H_{ortho}) orbital, whereas Lp(OP) and the vacant σ^*(N–H) orbital strengthen NH…OP hydrogen bond between the proton of the 4-FC_6H_4NH and the phosphoryl O atom. Stabilization energies E^2 of 4.7 and 8.2 kJ mol^{-1} were obtained for the Lp(OC) → σ^*(C–H_{ortho}) interaction in conformers **15a** and **15b**, respectively, whereas those of Lp(OP) → σ^*(N–H) interaction were calculated as 21.1 and 40.0 kJ mol^{-1}. At the same level, AIM analysis reveals charge density (ρ) values at the bcp of the CH…OC and NH…OP contacts in 0.0177 and 0.0321 e $Å^{-3}$. The ρ value at the ring critical point (rcp) for the O–C–N–C–C–H and O–P–N–C–N–H six-membered rings (Fig. S1) is 0.0114 and 0.0138 e $Å^{-3}$. This values confirm the formation of weak and strong interactions for CH…OC and NH…OP contacts.

Electronic parameters of the hydrogen-bonded clusters

For the compound **15**, the conformers were modeled as hydrogen-bonded clusters in which the target molecule (**A**) is surrounded by the same conformer (**A′**) and two neighbors (**B**, **B′**) (Fig. 5). The electronic parameters of the hydrogen-bonded clusters of compound **15** were calculated by AIM and NBO methods. The results of AIM and NBO analyses for H-optimized clusters are presented in Table 6. The bond lengths in optimized clusters are equal to those obtained for X-ray structures (Table S1), except for C–H and N–H bonds, since the optimizations have only been performed for H atom positions. Also, the donor–acceptor distances for hydrogen bonds in model clusters are equal to the experimental values. NBO analysis reveals [LP(O_C) → σ^*(N–H)] and [Lp(O_P) → σ^*(N–H)] interactions among the subunits within the clusters. This electronic delocalization leads to the weakening of the N–H bond. This is in good agreement with the decrease in the ρ value at the bcp of the N–H bond from the monomers to their corresponding clusters (Table 6 and S1). Moreover, the D–H–A angles in the optimized clusters are more linear than those in the solid-state structures. These indicate that the hydrogen bonds in the optimized clusters are stronger than those in the X-ray structures. It has been previously explained that the charge density at the bcp of DH…A increased when the donor–acceptor distance shortens. The results of AIM analysis show that ρ value at bcp of intramolecular hydrogen bond **A**(NH)…(O_P)-**A** (0.0362 e $Å^{-3}$) is larger in magnitude than that calculated for the intermolecular hydrogen bonds, i.e., **A**(NH)…(O_P)-**B** (0.0277 e $Å^{-3}$), **B′**(NH)…(O_P)**A** (0.0221 e $Å^{-3}$), and **A′**(NH)…(O_C)**A** (0.0266 e $Å^{-3}$). The smaller ρ values at the bcp of the N–H bond confirm the presence of the stronger interaction in intramolecular hydrogen bond in comparison with intermolecular hydrogen bonds. This is in good agreement with stabilizing energies $E^{(2)}$ for the title electronic delocalization in the model cluster. The stabilizing energies $E^{(2)}$ of 29.8 and 25.1 kJ mol^{-1} have been calculated for LP(O_P) → σ^*(N–H) electron density transfer in $(O_P)_B$ …H_A–N_A and $(O_P)_A$…$H_{B'}$–$N_{B'}$ hydrogen bonds, while it is 41.1 kJ mol^{-1} in the electronic delocalization LP(O_C) → σ^*(N–H) in the case of $(O_C)_A$ …$H_{Á}$–$N_{Á}$. Furthermore, the stabilizing energy E^2 of 45.6 kJ mol^{-1} has been calculated for LP(O_P) → σ^*(N–H) in $(O_P)_A$ …H_A–N_A hydrogen bond. This is in agreement with the values of distance for these hydrogen bonds in N_A–H_A…O_A–P_A (2.722(2)Å), $(O_P)_B$…–H_A–N_A (2.933(2)Å), $(O_P)_A$…$H_{B'}$–$N_{B'}$ (3.040(2)Å), $(O_C)_A$ …$H_{Á}$–$N_{Á}$ (2.969(2)Å) models. Besides, the hydrogen-bonding energy in the $(O_P)_B$ …H_A–N_A and $(O_P)_A$…$H_B$$N_B$ models (−9.7 and −7.1 kJ mol^{-1}) is smaller than the value calculated for $(O_C)_A$ …$H_{Á}$–$N_{Á}$ (−39.9 kJ mol^{-1}) model. It should be noted that the stabilizing energies $E^{(2)}$ differ from the hydrogen-bonding energy. The hydrogen-bonding energy is related to the sum of the total attractive and repulsive forces between two hydrogen-bonded fragments, and E^2 refers to the stabilization energy of electronic delocalization between the donor–acceptor orbital.

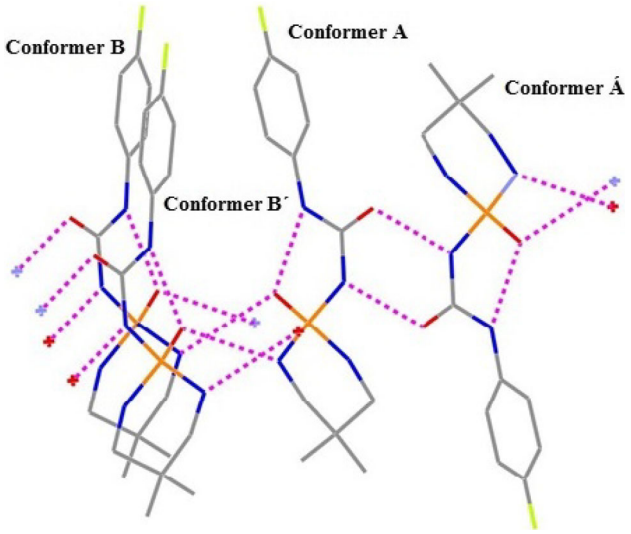

Fig. 5 Model hydrogen-bonded cluster for DFT calculations, in which the target molecule (**conformer A**) is in the center. A similar model was considered for the cluster in which conformer B in the center is the target molecule

QSAR analysis

In order to understand the observed pharmacological properties of the investigated analogs and determine the crucial factors governing these activities, QSAR studies were undertaken. The stepwise MLR procedure was used for model selection, which is a common method used in QSAR studies. Therefore, experimental IC_{50} values of 22 tested compounds with the general formula of $RC_6H_5(NH)^1C(O)(NH)^2P(O)R_1R_2$ (**13–34**), phenylurea, and **CP** were employed for constructing QSAR models against five data sets corresponding to the five tested cell lines, i.e., MDA-MB-231, PC-3, MCF-7, K562, and HeLa. For each data set, compounds with inactive cytotoxic activity were excluded from the analysis. For example, compound **30** was identified as an outlier for the MDA-MB-231 model and was subjected to removal, whereas none of the outliers were identified in MCF-7 model. The electronic and structural descriptors were obtained by quantum chemical calculations (Table 7). An optimal QSAR equation based on experimental data (δ, log P, and Mr) shown in Table 2 (eq. a), as well as eq. b is produced by replacement of experimental variables with the descriptors derived from the DFT calculations. Afterward, PCA method was used to reduce the independent variables (Pillai *et al*., 2005). The variable selection in PCA was performed by using the Fisher's weights approach (Molfetta *et al*., 2005), and the results are summarized as the following Eqs. (1, 2).

$$\begin{aligned} PC_1 = {} & 0.346\,E_h + 0.330E_l + 0.338E_{l+1} + 0.301E_{h-1} \\ & - 0.326W + 0.063Q_p - 0.303Q_{N2} - 0.236Q_C \\ & - 0.187PL_{P=O} - 0.117\ PL_{(N\{--\}H)1} \\ & - 0.269PL_{(N\{--\}H)2} - 0.213M_V + 0.235T_E \end{aligned} \quad (1)$$

$$\begin{aligned} PC_2 = {} & 0.001\,E_h - 0.005\,E_l - 0.034\,E_{l+1} - 0.054\,E_{h-1} \\ & - 0.033W + 0.514Q_p - 0.212\,Q_{N2} - 0.362\,Q_C \\ & - 0.437\ PL_{P=O} + 0.224\ PL_{(N\{--\}H)1} \\ & + 0.178\,PL_{(N\{--\}H)2} + 0.299\,M_V - 0.311\,T_E \end{aligned} \quad (2)$$

The main variables were found from the principle scores of the normalized eigenvalue of the two principal components. The results showed that the first and second factor PC on the total variance were 46.7 and 18.3 %, respectively. Also, from the above equations, it was deduced that the electronic parameters E_{HOMO}, E_{LuMO}, W, Q_P, Q_C, Q_{N2}, $PL_{P=O}$, PL_{N-H}, and T_E predominated over those related to structural parameter (Mv).

MDA-MB-231 model

The MLR was performed using these thirteen descriptors and equations are shown in Table S2. This method led to an optimal QSAR Eq. 3:

$$\begin{aligned} Log(1/IC_{50}) = {} & 14.350E_{H-1} + 0.006W - 1.078Q_P \\ & + 77.247Q_C + 13.463PL_{(N\{--\}H)1} \\ & - 28.317PL_{(N\{--\}H)2} - 83.257 \end{aligned} \quad (3)$$

Table 6 Hydrogen bond data for the X-ray structure (values in brackets), model cluster (at B3LYP/6-311+G**), charge densities (from AIM analysis), and delocalization energy (from NBO)

D–H…A	*d*(N–H)	*d*(H…O)	*d*(N…O)	<(NHO)	ρ(a.u.)		SE	ΔE_{HB}
					bcp1	bcp2		
N(2A)–H(2NA)…O(1)^{i}	[0.860]1.024	[2.20]2.02	3.040(2)	[168.0]176.3	0.3166	0.0221	[25.2]	[−7.1]
N(2)–H(2N)…O(1A)^{ii}	[1.00]1.024	[1.94]1.91	2.933(2)	[171.0]173.3	0.3172	0.0277	[29.8]	[−9.7]
N(3)–H(3 N)…O(2)^{iii}	[0.92]2.969	[2.05]1.94	2.969(2)	[175.0]175.9	0.3134	0.0264	[41.1]	[−39.9]
N(4)–H(4 N)…O(1)^{ii}	[0.82]2.722	[2.01]1.82	2.722(2)	[145.0]144.9	0.3235	0.0362	[45.6]	–

Symmetry codes: (i) $x, y - 1, z$; (ii) x, y, z; (iii) $-x, -y + 1, -z$. SE is the stabilizing energy $E^{(2)}$ (in kJ mol^{-1}) for the [$LP(O_C) \rightarrow \sigma^*(N–H)$] and [$Lp(O_P) \rightarrow \sigma^*(N–H)$] electronic delocalization. The binding energy is in kJ mol^{-1} for hydrogen bonds

ρ is the calculated charge density at the bcp of the D–H bond (bcp1) and H…A contact (bcp2) in the cluster

Table 7 Experimental and quantum chemical descriptors for derivatives **13–34**, cyclophosphamide (**CP**), and phenylurea computed at B3LYP/6-311+G** level

Comp.	Electronic																	Lipophilic		Steric	
	$\delta(^{31}P)$	$\delta(^{13}C)$	$\delta(NH)_1$	$\delta(NH)_2$	E_{HOMO}(a.u)	E_{LOMU}	E_l-E_h	E_{l+1}	W	Q(p)	$Q(N_1)$	$Q(N_2)$	Q(C)	PL(P=O)	PL (C=O)	PL $(N–H)_1$	PL $(N–H)_2$	Mr	μ(Debye)	Log P	M_V (Cm^3/mol)	T_E
13	3.78	153.30	9.32	7.63	−0.218	−0.024	0.193	−0.010	0.076	2.332	−0.640	−1.009	0.819	−3.407	−1.472	−1.078	−1.422	5.879	6.362	3.181	184.975	−1179.89
14	3.85	153.30	9.22	7.58	−0.210	−0.024	0.187	−0.008	0.073	2.332	−0.640	−1.010	0.818	−3.407	−1.474	−1.076	−1.422	6.227	5.819	3.326	195.836	−1219.22
15	3.23	156.40	9.37	7.75	−0.260	−0.101	0.159	−0.046	0.205	2.313	−0.615	−0.971	0.824	−3.409	−1.475	−1.078	−1.421	6.803	9.236	2.998	167.385	−1279.16
16	3.72	153.10	10.06	7.92	−0.219	−0.026	0.193	−0.020	0.078	2.333	−0.640	−1.008	0.819	−3.347	−1.472	−1.002	−1.374	6.170	8.304	2.812	249.760	−1384.45
17	3.60	153.39	9.47	7.75	−0.236	−0.051	0.287	−0.032	0.072	2.335	−0.639	−1.002	0.822	−3.411	−1.468	−1.080	−1.416	6.209	12.583	2.631	193.491	−1272.16
18	4.62	153.44	9.19	7.91	−0.215	−0.024	0.191	−0.010	0.074	2.332	−0.639	−1.010	0.819	−3.407	−1.472	−1.076	−1.422	6.227	6.003	3.326	212.435	−1219.22
19	3.41	153.49	9.35	7.70	−0.240	−0.094	0.146	−0.032	0.192	2.335	−0.641	−1.003	0.822	−3.411	−1.473	−1.080	−1.421	6.803	10.690	2.998	221.609	−1279.16
20	3.80	153.50	9.85	8.50	−0.225	−0.027	0.198	−0.019	0.080	2.335	−0.640	−1.008	0.821	−3.409	−1.475	−1.084	−1.417	6.170	7.875	2.812	215.605	−1384.46
21	4.62	153.44	9.21	6.86	−0.214	−0.024	0.190	−0.010	0.075	2.332	−0.649	−1.009	0.820	−3.407	−1.472	−1.091	−1.422	6.227	6.430	3.326	206.004	−1219.22
22	2.86	153.53	9.35	7.67	−0.247	−0.097	0.148	−0.034	0.202	2.320	−0.645	−0.989	0.829	−3.398	−1.476	−1.094	−1.416	6.803	5.521	2.999	159.589	−1279.16
23	3.79	153.40	10.19	8.51	−0.224	−0.024	0.199	−0.019	0.077	2.331	−0.642	−1.003	0.821	−3.367	−1.474	−1.101	−1.409	6.170	5.909	2.812	218.974	−1384.45
24	23.54	153.00	9.52	7.52	−0.219	−0.022	0.197	−0.012	0.074	2.290	−0.638	−0.999	0.823	−3.370	−1.469	−1.075	−1.426	4.994	6.530	2.021	172.630	−1061.92
25	23.65	153.00	9.42	7.50	−0.212	−0.021	0.191	−0.009	0.071	2.290	−0.637	−1.000	0.822	−3.370	−1.470	−1.074	−1.426	5.342	6.060	2.166	157.135	−1101.25
26	23.30	156.43	9.55	7.58	−0.247	−0.091	0.156	−0.033	0.183	2.293	−0.636	−0.992	0.826	−3.372	−1.469	−1.076	−1.425	5.915	12.896	1.838	189.388	−1161.19
27	23.58	152.80	10.19	7.83	−0.221	−0.024	0.197	−0.021	0.076	2.291	−0.638	−0.998	0.822	−3.372	−1.460	−1.077	−1.421	5.285	8.340	1.652	190.263	−1266.49
28	23.53	153.03	9.65	7.62	−0.238	−0.053	0.185	−0.031	0.114	2.292	−0.638	−0.993	0.825	−3.372	−1.463	−1.078	−1.421	5.323	12.314	1.471	224.670	−1154.19
29	24.10	153.24	9.38	7.81	−0.216	−0.022	0.194	−0.011	0.073	2.290	−0.637	−1.000	0.823	−3.370	−1.468	−1.074	−1.426	5.342	6.380	2.166	155.274	−1101.25
30	23.53	153.13	9.54	7.56	−0.243	−0.096	0.147	−0.034	0.196	2.292	−0.639	−0.993	0.825	−3.371	−1.466	−1.077	−1.424	5.915	9.590	1.838	170.167	−1161.19
31	23.58	153.10	9.50	7.52	−0.228	−0.024	0.203	−0.022	0.078	2.291	−0.638	−0.997	0.824	−3.370	−1.468	−1.081	−1.421	5.285	7.360	1.652	193.258	−1266.48
32	24.12	153.24	9.21	7.31	−0.215	−0.023	0.193	−0.015	0.073	2.291	−0.646	−1.000	0.825	−3.372	−1.470	−1.088	−1.427	5.342	6.830	2.166	173.579	−1101.24
33	22.94	153.16	9.54	7.58	−0.246	−0.096	0.150	−0.034	0.196	2.283	−0.653	−0.985	0.827	−3.359	−1.470	−1.092	−1.421	5.915	5.370	1.838	168.863	−1161.18
34	23.66	153.06	10.30	8.39	−0.225	-0.022	0.204	−0.020	0.075	2.288	−0.640	−0.994	0.824	−3.340	−1.468	−1.120	−1.412	5.285	5.631	1.652	186.018	−1266.48
CP	11.53	–	–	–	−0.268	−0.025	0.243	−0.010	0.088	2.394	–	–	–	−3.450	–	–	–	3.443	5.186	2.739	157.513	−1797.78
Phenylurea	–	156.08	8.53	5.88	−0.227	−0.023	0.250	−0.017	0.062	–	−0.626	−0.836	0.799	–	−1.451	−1.006	−1.242	1.853	4.204	1.320	107.774	−456.45

QSAR descriptors include chemical shift (δ), energy of highest occupied and lowest unoccupied molecular orbital (E_{HOMO} and E_{LUMO}), after highest occupied and next lowest unoccupied molecular orbital (E_{H-1} and E_{L+1}), energy difference between the LUMO and HOMO ($\Delta E_{L–H}$), electrophilicity (w), polarizability (PL), net atomic charge (Q), hydrophobic coefficient (log P), dipole moment (μ), molecular volume (Mv), and molecular total energy (TE)

$n = 16$; $R^2 = 0.939$; $R^2_{adj} = 0.885$; $F = 17.497$; $S_{reg} = 0.103$

In this equation, the inhibitory potency of MDA-MB-231 cell line is influenced mainly by the electronic parameters. Qc with the coefficient values of +77.247 has the highest contribution to log ($1/IC_{50}$) rather than the other electronic parameters such as the net charge of P=O phosphorus (−1.078). The positive coefficient associated with the parameter Qc suggests that increases in the negative charge or electron density at the C=O carbon may be favorable to higher antitumor activity against MDA-MB-231 cell line. The correlation matrix was used to determine the interrelationship between the independent variables (Table 8). The high interrelationship observed between Q_C descriptor and W ($r = +0.721$) showed that electrophilicity properties of the studied derivatives affect the inhibition of human MDA-MB-231. Compounds **16** ($W = 0.205$) and **36** ($W = 0.062$) are in order of the highest and the lowest inhibitory potentials.

MCF-7 model

Besides net charge of the N–H nitrogen Q_{N2}, E_H properties of compounds are highly involved in cytotoxic activity against the MCF-7 cell line as shown by the QSAR equation below:

$$\mathrm{Log}(1/\mathrm{IC}_{50}) = 10.13E_H - 2.702E_{H-1} - 10.201Q_{N2} - 5.699\mu + 0.019\mathrm{PL}_{(P=O)} + 0.001\mathrm{PL}_{(C=O)} + 1.705 \quad (4)$$

$n = 11$; $R^2 = 0.939$; $R^2_{adj} = 0.885$; $F = 17.497$; $S_{reg} = 0.103$

Q_{N2} and E_H with the coefficient values of −10.201 and 10.130 have the highest contribution to log ($1/IC_{50}$) rather than the structural parameters. The negative and positive signs of Q_{N2} and E_H in log ($1/IC_{50}$) disclose that the compound with lower net charge Q_{N2} and higher molecular orbital E_H is indicative of higher potency against MCF-7 cell line. The interrelationships between the variables and the correlation matrix results are presented in Table S3. The high and low interrelationships were observed between Q_{N2} and $PL_{C=O}$ ($r = -0.840$), and Q_{N2} and E_H ($r = -0.325$), respectively. The high interrelationship between Q_{N2} and $PL_{C=O}$ ($r = -0.840$) shows that $PL_{C=O}$ controls the effect of net charge of the N–H nitrogen Q_{N2} on the inhibition of the titled cell line. Diazaphosphorinane with fluorine substituent at *ortho* position **22** ($PL_{C=O} = -1.476$) and phenylurea **36** ($PL_{C=O} = -1.451$) are in order of the highest and the lowest inhibitory potentials against MCF-7 cell line.

PC-3 and HeLa models

Similar results were found in both PC-3 and HeLa models in which the electronic descriptors were governing the cytotoxic activity. The QSAR equation of the PC-3 model is shown below:

$$\mathrm{Log}(1/\mathrm{IC}_{50}) = -27.559E_{L+1} - 8.847E_{H-1} + 26.613W + 343.388Q_{N2} + 8.79Q_C + 1.586\mu - 0.004\ \mathrm{PL}_{(P=O)} - 335.95 \quad (5)$$

$n = 11$; $R^2 = 0.965$; $R^2_{adj} = 0.883$; $F = 11.814$; $S_{reg} = 0.034$

In Eq. (5), Q_{N2} representing the net charge of the N–H nitrogen seems to be the most important descriptor as deduced from its highest regression coefficient value of 343.388. High colinearity ($r > 0.5$) was observed between different parameters (Table S4). The high interrelationship was observed between Q_{N2} and W ($r = -0.841$), and low interrelationship was observed between this descriptor and $PL_{P=O}$ ($r = 0.087$). From the correlation matrix, it was observed that the electrophilicity (W) was found to be most effective in describing the anticancer activity of the

Table 8 Correlation matrix for log ($1/IC_{50}$) and selected parameters in Eq. 3

Selected variables	MDA-MB-231						
	E_{H-1}	W	Q_P	Q_C	$PL_{(N-H)1}$	$PL_{(N-H)2}$	M_v
E_{H-1}	1						
W	−0.814	1					
Q_P	0.283	−0.215	1				
Q_C	−0.640	0.721	−0.675	1			
$PL_{(N-H)1}$	−0.201	0.115	0.089	−0.166	1		
$PL_{(N-H)2}$	−0.509	0.635	0.140	0.318	0.650	1	
M_v	−0.422	0.511	0.258	0.175	0.452	0.587	1

synthesized compounds. As shown in Table 7, compounds **16** and **36** with electrophilicity (W) values 0.205 and 0.062 have the highest and the lowest inhibitory potentials against the titled cell line.

The QSAR equation of the HeLa model is shown below:

$$\begin{aligned}\mathrm{Log}(1/\mathrm{IC}_{50}) = {} & 10.13E_H - 6.661E_{H-1} + 261.821Q_{\mathrm{N2}} \\ & + 50.015\mu + 0.012\mathrm{PL}_{(\mathrm{P=O})} \\ & - 0.007\mathrm{PL}_{(\mathrm{C=O})} - 155.829 \qquad (6)\end{aligned}$$

$$n = 11;\ R^2 = 0.86;\ R^2_{\mathrm{adj}} = 0.651;\ F = 4.105;\ S_{\mathrm{reg}} = 0.095$$

Similarly the model described by Eq. 6 showed that the most effective variable in the inhibition of HeLa cell line by the tested derivatives was Q_{N2}, with the coefficient value of 261.821. The interrelationships between the variables and the correlation matrix results are presented in Table S5. A high interrelationship was observed between Q_{N2} and E_{H} ($r = -0.758$). Compounds **14** ($E_{\mathrm{H}} = -0.2105$) and **35** ($E_{\mathrm{H}} = -0.268$) are in order of the highest and the lowest inhibitory potentials. The positive coefficients of Q_{N2} at Eqs. 5 and 6 indicate that the increase in the negative charge or electron density at the N–H nitrogen may be favorable to higher antitumor activity.

K562 model

Distinct from other cell lines, the cytotoxic activity of compounds against the K562 cell line is dependent on the next lowest unoccupied molecular orbital shown in the equation below:

$$\begin{aligned}\mathrm{Log}(1/\mathrm{IC}_{50}) = {} & 22.06E_{L+1} - 3.1E_{H-1} + 7.877Q_{\mathrm{N2}} \\ & + 3.078\mu + 0.004\mathrm{PL}_{(\mathrm{P=O})} + 0.281 \qquad (7)\end{aligned}$$

$$n = 12;\ R^2 = 0.941;\ R^2_{\mathrm{adj}} = 0.869;\ F = 13.193;\ S_{\mathrm{reg}} = 0.006$$

It can be seen that the $E_{\mathrm{L+1}}$ descriptor is responsible for prediction of the cytotoxic activity of K562 cell line as deduced from its high regression coefficient value of 22.06. The positive sign of $E_{\mathrm{L+1}}$ in log ($1/\mathrm{IC}_{50}$) discloses that the compound with higher molecular orbital ($E_{\mathrm{L+1}}$) may be conducive to the biological activity of these diazaphosphore compounds. The correlation matrix of different descriptors used in the QSAR models is shown in Table S6. The high interrelationship was observed between $E_{\mathrm{L+1}}$ and $E_{\mathrm{H-1}}$ ($r = -0.553$), and low interrelationship was observed for Q_{N2} ($r = -0.01$). Then, compound **21** having high $E_{\mathrm{H-1}}$ value (−0.240) displayed high anticancer activity. Similarly, compound **27** having low $E_{\mathrm{H-1}}$ value (−0.277) exhibited low anticancer potential. Obtained results from the above data can be summarized as follows:

1. QSAR studies demonstrated that cytotoxic activities of compounds **13–34**, **CP**, and phenylurea against the investigated cell lines were influenced by the electronic descriptors. This indicates that such distinct chemical properties are crucial for the cytotoxic activity against particular cell lines.
2. QSAR studies also emphasize that higher probability of electrophilic attack at the nitrogen atom number 2 may be favorable to the biological activity compared to the nitrogen atom number 1. This is in agreement with the values of the electron density (ρ) for nitrogen atom in two amidic (8.383 $\mathrm{e\AA^{-3}}$) and aniline (8.174 $\mathrm{e\AA^{-3}}$) bonds obtained by AIM analysis. This may explain much interaction N_1 with neighbor groups compared to the N_2 atom. NBO analysis reveals an [Lp(N) σ^*(C=O)] interaction with the stabilizing energies E^2 of 56.99 and 32.39 kcal $\mathrm{mol^{-1}}$ for lone pair N_1 and N_2, respectively. This electronic delocalization leads to reduction in the (ρ) value for nitrogen atom from N_2–H bond to N_1–H bond.
3. Net charge of the N–H nitrogen (Q_{N2}) seemed to be important descriptor for the cytotoxic activity against MCF-7, PC-3, and HeLa cell lines, whereas net charge of the C=O carbon (Qc) and $E_{\mathrm{L+1}}$ were shown to be crucial for MDA-MB-231 and K562, respectively. With respect to importance of the electronic descriptors against the studied cell lines, it could be hypothesized that the mechanism of cytotoxic activity of diazaphosphore compounds may be similar.
4. Experimental and theoretical data demonstrate the importance of six-membered ring for cytotoxicity. This might be explained by the electronic nature of phosphor atom.

Validation of QSAR

In each cell lines, a set of compounds was used as a training set for QSAR modeling. The remaining compounds were adopted as a test set for validating the QSAR model. Considering the balance of the QSAR quality and the number of employed quantum chemical descriptors, an optimal equation was achieved for the selected compounds in the training set by MLR analysis for the studied cell lines (Table S7). The developed QSAR models were cross-validated with q^2 value ($q^2 > 0.5$) obtained by leave-one-out (LOO) method. The value of q^2 more than 0.5 indicates that the model developed is a valid one. According to the recommendations of Golbraikh and Tropsha, the only way to estimate the true predictive power of a model is to test their ability to predict accurately the biological activities of compounds. As the observed and predicted values are close

Table 9 External validation for the established QSAR models of MDA-MB-231, MCF-7, PC-3, HeLa, and K562 human tumor cell lines

Com.	MDA-MB-231			MCF-7			PC-3			HeLa			K562		
	Meas	Pred	Res	Meas	Pred	Res	Mea	Pred	Res	Mea	Pred	Res	Mea	Pred	Res
13	−0.616	−0.607	0.009	−0.792	0.334	1.126	−1.472	−1.357	0.115	−0.522	−0.520	0.002	−0.677	1.646	2.323
14	−0.471	−0.657	−0.186	−0.366	0.605	0.971	−0.704	−1.483	−0.779	−0.814	−0.307	0.506	−0.617	2.057	2.674
15	−0.724	−0.872	−0.149	−0.596	0.685	1.280	−0.538	−2.530	−1.993	−0.484	−0.412	0.072	−0.912	1.454	2.367
16	−0.826	6.550	7.376	−0.951	−2.462	−1.512	−0.450	1.102	1.552	–	–	–	−0.859	−3.551	−2.690
17	0.310	−0.108	−0.418	−0.742	−0.1423	0.600	−0.428	−1.052	−0.624	−0.681	−0.773	−0.092	−1.060	−1.102	−0.042
18	−0.352	−0.266	0.086	−0.124	0.001	0.125	−0.041	0.308	0.349	−0.182	−0.470	−0.284	−0.215	−0.164	0.051
19	−0.481	−0.217	0.265	−0.680	−0.242	0.435	−0.864	−0.464	0.399	−0.544	−0.575	−0.031	−0.989	−0.930	0.059
20	−0.720	−0.802	−0.082	−0.934	−0.448	0.486	−0.590	−1.214	−0.624	−0.745	−0.620	0.126	–	–	–
21	−0.425	−0.676	−0.250	−0.328	−0.111	0.217	−0.350	0.450	0.800	−0.322	−0.380	−0.058	−0.584	−0.475	0.110
22	−0.678	−0.403	0.276	−0.497	−0.218	0.280	−0.603	−1.051	−0.448	−1.248	−0.101	1.147	−0.653	−0.038	0.615
23	−0.671	0.576	1.254	−0.751	−0.965	−0.213	−0.600	−0.838	−0.241	−0.521	0.000	0.521	−0.450	−0.528	−0.078
24	0.168	−0.277	−0.445	−0.908	−0.068	0.841	−1.478	−1.357	0.121	−0.808	−0.134	0.673	–	–	–
25	−0.747	−0.365	0.383	−0.985	0.236	1.221	−1.145	0.080	1.224	–	–	–	–	–	–
26	−0.733	−0.809	−0.076	−1.221	0.439	1.660	−1.264	−1.326	−0.062	−0.628	−0.174	0.455	−0.669	1.398	2.068
27	−0.303	−0.443	−0.140	−0.107	−0.582	−0.475	−0.413	0.308	0.721	−0.462	−0.888	−0.426	–	–	–
28	−0.453	−0.366	0.088	−0.228	−0.227	0.001	−0.228	−0.197	0.0313	−0.487	−0.579	−0.092	–	–	–
29	0.056	0.0247	−0.031	0.143	−0.384	−0.526	−0.241	1.536	1.777	−0.130	−0.115	0.015	−0.477	−0.520	−0.043
30	–	–	–	−1.206	−0.218	0.280	−0.612	0.541	1.153	–	–	–	−0.765	−1.192	−0.427
31	−0.953	−0.781	0.172	−0.760	−0.461	0.299	−0.816	−0.871	−0.055	−1.477	−0.477	1.000	–	–	–
32	−0.146	−0.208	−0.062	−0.825	−0.520	0.306	−0.784	2.160	2.944	−0.731	0.007	0.737	−0.608	−0.713	−0.106
33	−0.217	−0.426	−0.208	−0.505	−0.392	0.114	–	–	–	–	–	–	–	–	–
34	−0.951	−1.029	−0.078	−1.245	−1.050	0.195	−0.647	−0.351	0.296	–	–	–	−1.315	−1.230	0.086
CP	−1.246	−1.247	−0.002	−0.892	−0.892	0	−1.178	−1.179	−0.001	−1.009	−1.009	0.001	−1.206	−1.210	−0.000
Phenylurea	−0.431	−0.424	0.007	−1.598	−1.598	0	−1.127	−1.128	−0.002	−0.851	−0.850	0.001	−1.615	−1.616	−0.001

to each other (Table 9), the QSAR models for anticancer activity are valid (Golbraikh and Tropsha, 2002).

Conclusion

In this study, new sixteen diazaphosphore derivatives, differing in the nature of the aliphatic and aromatic rings, were synthesized and investigated for their biological activity. Novel anticancer agents **18** and **29** with methyl group at *meta* position of aromatic ring exhibited higher cytotoxic activity against most of tested cell lines than other derivatives which may be due to size, steric, and electronic properties of the substituent. The models obtained through QSAR study gave a better prediction capability of anticancer activity against the studied human cell lines. Electronic parameters such as Q_{N2}, QC, and E_{L+1} were major factors responsible for positively affecting the anticancer activity of the selected diazaphosphore derivatives. As evident from the experimental and QSAR data, the presence of six-membered ring of diazaphosphore is essential for higher antitumor activity. Besides, important of the nitrogen atom number 2 at anticancer activity compared with the nitrogen atom number 1 expressed by result of NBO and AIM analysis. Comparison of the results of antibacterial studies exhibited further emphasis on the importance of six-membered diaza ring in addition to the requirement of substitutions in the aromatic ring.

Supplementary data

Crystallographic data for structure **15** have been deposited with the Cambridge Crystallographic Data Centre as supplementary publication Nos. CCDC 1428625 ($C_{12}H_{18}F_1N_4O_2P$). Copies of the data may be obtained free of charge upon request from CCDC, 12 Union Road, Cambridge CB2 1EZ, UK (fax: +44 1223 336033; E-mail: deposit@ccdc.cam.ac.uk or www: http://www.ccdc.cam.ac.uk

Acknowledgments The financial support of this work provided by the Research Council of Tarbiat Modares University and the Razi Herbal Medicines Research Centre of Lorestan University of Medical Sciences is gratefully acknowledged.

References

Barry AL (1977) The Antimicrobial susceptibility test; principle and practice. Bio Abstr 64:25183

Borch RF, Canute GW (1991) Synthesis and antitumor properties of activated cyclophosphamide analogues. J Med Chem 34:3044–3052

Boys SF, Bernardi F (1970) The calculation of small molecular interactions by the differences of separate total energies. Some procedures with reduced errors. Mol Phys 19:553–566

Bøyum A (1976) Isolation of lymphocytes, granulocytes and macrophages. Scand J Immunol 5:9–15

Breitmaier E, Voelter W (1990) Carbon-13 NMR spectroscopy. VCH, Weinheim, New York, pp 143, 153

Bruker S (1998) Bruker molecular analysis research tool, version 5.059, Bruker AXS: Madison, WI

Carletti E, Colletier JP, Dupeux F, Trovaslet M, Masson P, Nachon F (2010) Structural evidence that human acetylcholinesterase inhibited by tabun ages through o-dealkylation. J Med Chem 53:4002–4008

Corbridge DEC (1995) Phosphorus, an outline of its chemistry, biochemistry and technology, 5th edn. Elsevier, The Netherlands, pp 55–57

Denmark SE, Su X, Nishigaichi Y, Coe DM, Wong KT, Winter SBD, Choi JY (1999) Synthesis of phosphoramides for the lewis base-catalyzed allylation and aldol addition reactions. J Org Chem 64:1958–1967

Elgorashi EE, Malan SF, Stafford GI, Staden JV (2006) Quantitative structure-activity relationship studies on acetylcholinesterase enzyme inhibitory effects of Amaryllidaceae alkaloids. S Afr J Bot 72:224–231

Esrafili MD, Elmi F, Hadipour NL (2007) Density functional theory investigation of hydrogen bonding effects on the oxygen, nitrogen and hydrogen electric field gradient and chemical shielding tensors of anhydrous chitosan crystalline structure. J Phys Chem A 111:963–970

Frisch MJ, Trucks GW, Schlegel HB, Scuseria GE, Robb MA, Cheeseman JR, Montgomery Jr JA, Vreven T, Kudin KN, Burant JC, Millam JM, Iyengar SS, Tomasi J, Barone V, Mennucci B, Cossi M, Scalmani G, Rega N, Petersson GA, Nakatsuji H, Hada M, Ehara M, Toyota K, Fukuda R, Hasegawa J, Ishida M, Nakajima T, Honda Y, Kitao O, Nakai H, Klene M, Li X, Knox JrE, Hratchian HP, Cross JB, Adamo C, Jaramillo J, Gomperts R, Stratmann RE, Yazyev O, Austin AJ, Cammi R, Pomelli C, Ochterski JW, Ayala PY, Morokuma K, Voth GA, Salvador P, Dannenberg JJ, Zakrzewski VG, Dapprich S, Daniels AD, Strain MC, Farkas O, Malick DK, Rabuck AD, Raghavachari K, Foresman JB, Ortiz JV, Cui Q, Baboul AG, Clifford S, Cioslowski J, Stefanov BB, Liu G, Liashenko A, Piskorz P, Komaromi I, Martin RL, Fox DJ, Keith T, Al-Laham MA, Peng CY, Nanayakkara A, Challacombe M, Gill PMW, Johnson B, Chen W, Wong MW, Gonzalez C, Pople JA (2003). GAUSSIAN03, Revision B. 03. Gaussian Inc., Pittsburgh, PA, USA

Gholivand K, Dorosti N (2011) Synthesis, spectroscopic characterization, crystal structures, theoretical studies, and antibacterial evaluation of two novel N-phosphinyl ureas. Monatsh Chem 142:183–192

Gholivand K, Dorosti N (2013) Some new compounds with P(E)NHC(O) (E = lone pair, O, S) linkage: synthesis, spectroscopic, crystal structures, theoretical studies, and antimicrobial evaluation. Monatsh Chem 144:1417–1425

Gholivand K, Shariatinia Z, Mahdieh S, Farzaneh Daeepour M, Farshidnasab N, Mahzouni HR, Taheri N, Amiri S, Ansar S (2009) Structural diversity in phosphoramidate's chemistry: syntheses, spectroscopic and X-ray crystallography studies. Polyhedron 28:307–321

Gholivand K, Dorosti N, Shariatinia Z, Ghaziany F, Sarikhani S, Mirshahi M (2010) Cyclophosphamide analogues: synthesis, spectroscopic study, and antitumor activity of diazaphosphorinanes. Med Chem Res 21:2185–2195

Gholivand K, Dorosti N, Ghaziany F, Mirshahi M, Sarikhani S (2012) N-Phosphinyl ureas: synthesis, characterization, X-ray structure, and in vitro evaluation of antitumor activity. Heteroatom Chem. 23:74–83

Gholivand K, Ebrahimi Valmoozi AA, Bonsaii M (2014) Synthesis, biological evaluation, QSAR study and molecular docking of

novel N-(4-amino carbonylpiperazinyl) (thio)phosphoramide derivatives as cholinesterase inhibitors. Pestic Biochem Physiol 112:40–50

Golbraikh A, Tropsha A (2002) Beware of q2! J Mol Graphics Model 20:269–276

Hansch C, Fujita T (1964) p-σ-π Analysis a method for the correlation of biological activity and chemical structure. J Am Chem Soc 86:1616–1626

Hocková D, Holý A, Andrei G, Snoeck R, Balzarini J (2011) Acyclic nucleoside phosphonates with a branched 2-(2-phosphonoethoxy) ethyl chain: efficient synthesis and antiviral activity. Bioorg Med Chem 19:4445–4453

Hua R, Doucet JP, Delamar M, Zhang R (2009) QSAR models for 2-amino-6-arylsulfonylbenzonitriles and congeners HIV-1 reverse transcriptase inhibitors based on linear and nonlinear regression methods. Eur J Med Chem 44:2158–2171

Jeffrey GA, Saenger W (1991) Hydrogen bonding in biological structures. Springer, Berlin

Jiang Y, Han J, Yu C, Vass SO, Searle PF, Browne P, Knox RJ, Hu L (2006) Design, synthesis, and biological evaluation of cyclic and acyclic nitrobenzylphosphoramide mustards for e. coli nitroreductase activation. J Med Chem 49:4333–4343

Kirsanov AV (1954) J Gen Chem USSR 24:1031

Kirsanov AV, Zhmurova IV (1956) J Gen Chem USSR 26:2642

Li Z, Han J, Jiang Y, Browne P, Knox RJ, Hu L (2003) Nitrobenzocyclophosphamides as potential prodrugs for bioreductive activation: synthesis, stability, enzymatic reduction, and antiproliferative activity in cell culture. Bioorg Med Chem 11:4171–4178

Ludeman SM, Zon G, Egan W (1979) Synthesis and antitumor activity of cyclophosphamide analogues. 2.1 Preparation, hydrolytic studies, and anticancer screening of 5-bromocyclophospha-mide, 3,5-dehydrocyclophosphamide, and related systems. J Med Chem 22:151–158

Mara C, Dempsey E, Bell A, Barlow JW (2011) Synthesis and evaluation of phosphoramidate and phosphorothioamidate analogues of amiprophos methyl as potential antimalarial agents. Bioorg Med Chem Lett 21:6180–6183

Massiah MA, Viragh C, Reddy PM, Kovach IM, Johnson J, Rosenberry TL, Mildvan AS (2001) Strong hydrogen bonds at the active site of human acetylcholinesterase: ^{1}H-NMR studies. Biochemistry 40:5682–5690

Mirzaei M, Elmi F, Hadipour NL (2006) A systematic investigation of hydrogen-bonding effects on the 17O, 14N, and 2H nuclear quadrupole resonance parameters of anhydrous and monohydrated cytosine crystalline structures: a density functional theory study. J Phys Chem B. 110:10991–10996

Mohe NU, Padiya KJ, Salunkhe MM (2003) An efficient oxidizing reagent for the synthesis of mixed backbone oligonucleotides via the H-phosphonate approach. Bioorg Med Chem 11:1419–1431

Molfetta FA, Bruni AT, Honório KM, da Silva ABF (2005) A structure–activity relationship study of quinone compounds with trypanocidal activity. Eur J Med Chem 40:329–338

Monteil M, Migianu-Griffoni E, Sainte-Catherine O, Di Benedetto M, Lecouvey M (2014) Synthesis and biological evaluation in HuH7 hepatocarcinom a cells. Eur J Med Chem 77:56–64

Moon K-Y, Shirota FN, Baturay N, Kwon Ch-H (1995) Chemically stable N-methyl-4-(alkylthio)cyclophosphamide derivatives as prodrugs of 4-hydroxycyclophosphamide. J Med Chem 38:848–851

Parr RG, Szentpaly LV, Liu S (1999) Electrophilicity index. J Am Chem Soc 121:1922–1924

Pillai AD, Rani S, Rathod PD, Xavier FP, Vasu KK, Padh H, Sudarsanam V (2005) QSAR studies on some thiophene analogs as anti-inflammatory agents: enhancement of activity by electronic parameters and its utilization for chemical lead optimization. Bioorg Med Chem 13:1275–1283

Pinto MFS, Romero OAS, Pinheiro JC (2001) Pattern recognition study of structure-activity relationship of halophenols and halonitrophenols against fungus T. mentagrophytes. J Mol Struct THEO CHEM. 539:303–310

Roy DR, Sarkar U, Chattaraj PK, Mitra A, Padmanabhan J, Parthasarathi R, Subramanian V, Van Damme S, Bultinck P (2006) Analyzing toxicity through electrophilicity. Mol Divers 10:119–131

Sharma SK, Kumar P, Narasimhan B, Ramasamy K, Mani V, Mishra RK, Majeed AA (2012) Synthesis, antimicrobial, anticancer evaluation and QSAR studies of 6-methyl-4-[1-(2-substituted-phenylamino-acetyl)-1H-indol-3-yl]-2-oxo/thioxo-1,2,3,4-tetrahydropyrimidin e-5-carboxylicacid ethylesters. Eur J Med Chem 48:16–25

Sheldrick GM (2008) SHELXTL V.5.10, Structure determination software suite, Bruker AXS. Madison, WI

Sun Q, Li RT, Guo W, Cui JR, Cheng TM, Ge ZM (2006) Novel class of cyclophosphamide prodrug: cyclophosphamide spiropiperaziniums (CPSP). Bioorg Med Chem Lett 16:3727–3730

Venkatachalam TK, Qazi S, Uckun FM (2006) Synthesis and metabolism of naphthyl substituted phosphoramidate derivatives of stavudine. Bioorg Med Chem 14:5161–5177

Vincent JG, Vincent HW (1944) Filter paper disc modification of the Oxford cup penicillin determination. Proc Soc Exp Biol Med 55:162–164

Viswanadhan VN (1989) Atomic physicochemical parameters for three dimensional structure directed quantitative structure-activity relationships. 4. Additional parameters for hydrophobic and dispersive interactions and their application for an automated superposition of certain naturally occurring nucleoside antibiotics. J Chem Inf Comput Sci 29:163–172

Voorde JV, Liekens S, McGuigan C, Murziani PGS, Slusarczyk M, Balzarini J (2011) The cytostatic activity of NUC-3073, a phosphoramidate prodrug of 5-fluoro- 20-deoxyuidine, is independent of activation by thymidinekinase and insensitive to degradation by phosphorolytic enzymes, the cytostatic activity of NUC-3073. Biochem Pharmacol 82:441–452